MULTISPECTRAL AND HYPERSPECTRAL IMAGES INVARIANT TO ILLUMINATION

by

Amin Yazdani Salekdeh
B.Sc., Sharif University of Technology, 2009

a Thesis submitted in partial fulfillment
of the requirements for the degree of
Master of Science
in the School
of
Computing Science

SIMON FRASER UNIVERSITY
Spring 2011

APPROVAL

Name: Amin Yazdani Salekdeh

Degree: Master of Science

Title of Thesis: Multispectral and Hyperspectral Images Invariant to Illumination

Examining Committee: Dr. Richard T. Vaughan
Chair

Dr. Mark S. Drew, Senior Supervisor

Dr. Ze-Nian Li, Supervisor

Dr. M. Stella Atkins, SFU Examiner

Date Approved: 18 April 2011

Declaration of
Partial Copyright Licence

Abstract

In this thesis a novel method is proposed that makes use of multispectral and hyperspectral image data to generate a novel photometric-invariant spectral image. For RGB colour image input, an illuminant-invariant image was constructed independent of the colour and intensity of the illuminant and of shading. To generate this image either a set of calibration images was required, or entropy information taken from a single image was used to develop the parameters necessary to produce the invariant. Nonetheless, generating an invariant image remains a complex and error-prone task for RGB image data. In contrast, for spectral images with many more spectral channels (i.e., for multispectral or hyperspectral image data) we show that photometric-invariant image formation is in essence greatly simplified. One of the requirements for forming an invariant is the necessity of narrowband-sensor sensors. Here this is the case, and we show that with the simple knowledge of peak sensor wavelengths we can generate a high-dimensional spectral invariant. The PSNR is shown to be high between the respective invariant spectral features for multispectral and hyperspectral images taken under different illumination conditions, showing lighting invariance for a per-pixel measure; and the s-CIELAB error measure shows that the colour error between the 3-dimensional colour images used to visualize the output invariant high-dimensional data is also small.

To my parents for their continuous support

"Thoughts are the shadows of our feelings – always darker, emptier and simpler."

— Friedrich Nietzsche, *philosopher (1844-1900)*

Acknowledgments

I want to use this opportunity to thank my supervisor Dr. Mark Drew for his support, encouragement, and patience during my course of studies. Without his invaluable insights and directions this work could not have been done. I want to express my greatest thanks to Dr. Greg Mori for many things he taught me during my graduate career. Learning *"Machine Learning"* with him was one of the greatest experiences in my career. I also want to thank Dr. Ze-Nian Li for his valuable comments. I should use this place to extend my thanks to Dr. Robert Woodham whose insights in Physics-based Image Processing was inspiring for me, also Arash Vahdat and my other colleagues in Vision and Media Lab for helpful comments and discussions, and the great working atmosphere.

Contents

List of Figures

List of Programs

Chapter 1

Introduction

This thesis is concerned with generating invariant spectral images that are invariant to lighting conditions and effects. The illumination effects to be removed in this work are shadows, shadings, specularities and illuminant colour. RGB is a popular format for storing colour images, representing each pixel with a triple (Red, Green, Blue). RGB images have 3 channels and each pixel lives ina 3-dimensional space. In this thesis by using "3-D image" I mean an image with 3 channels, such as RGB images. On the other hand, spectral images usually have more than 3 channels.

Spectral images are divided into two groups in this thesis: First "multispectral' images which have more than 3 channels, up to about 31 channels, Second "hyperspectral" images, typically produced by airborne or space-borne remote sensing imaging systems and contain hundreds of narrowband channels. An important property of multispectral images is that all of the channels are in the visible domain for the human visual system. However, for hyperspectral images, many channels could be beyond the visible for the human visual system.

A typical camera has sensors which are broadband. Figure 1.1(a) shows a Kodak DCS420 camera sensors. As you can see many wavelengths contribute in each sensor. On the other hand for a narrowband sensor, only small group of wavelengths contribute in the response; in ideal format only one wavelength. Figure 1.1(b) shows an ideal camera with delta-like function sensors.

The thesis sets out a generalization to spectral images of previous work carried out on 3-dimensional image data in colour, R,G,B. In that previous work, an illumination invariant greyscale image was produced by reducing the dimensionality from 3 to 1 in stages, by progressively removing the influence of lighting in each step. The first step removes the shading and intensity by forming the band-ratio chromaticity which will reduce dimensionality of data from 3 to 2. The second step is to take a log of chromaticity to have the result linearized in illumination colour. Finally, the last step is to project the data into a specific direction which will result in removing effects of illumination effects and reducing the dimensionality from 2 to 1.

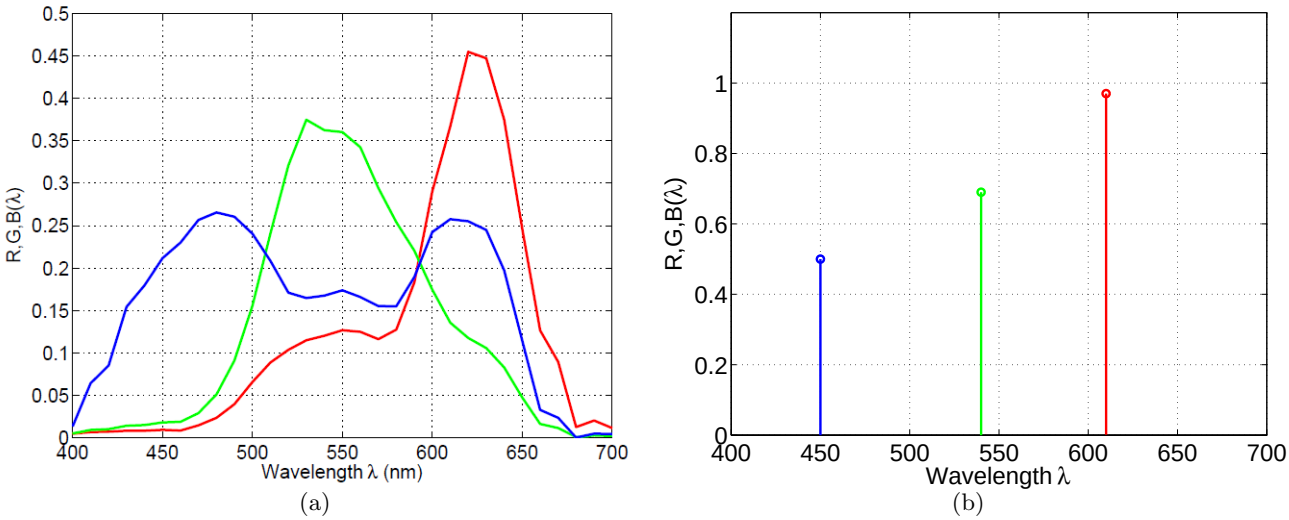

Figure 1.1: (a): Kodak DSC 420 camera with broadband sensors; (b): Ideal delta-like function camera

However, the final step, which removed the effect of lighting completely or at least greatly attenuated it, necessitated a camera calibration, in one embodiment, or somewhat less reliable use of entropy minimization as a mechanism for obtaining the final projection in a 2-space which generated the final greyscale.

Here, because of the special conditions under which higher-dimensional image data is typically obtained, we show that in fact the calibration or entropy minimization step can be omitted, thus greatly simplifying the algorithm. As a consequence, we show that it is possible to generate an illumination invariant for such higher-dimensional data using the new proposed method, with provable diminishment of the influence of light on such images. For example, quite striking results are obtained for "seeing into the shadows" for satellite images. Because of the availability of spectral data, it is also possible to visualize such results in RGB, thus creating a new mechanism for information display for high-dimensional images.

Since this work touches upon the related topics of colour constancy and 3-dimensional illumination invariant images, as well as the many proposed methods proposed for shadow identification and removal, these research directions are reviewed below. To begin, however, we introduce the framework for image formation utilized.

1.1 Light and Surface

1.1.1 Illuminant Spectral Power Distribution

Whereas in Computer Graphics light colour is simply taken as RGB triples, a fuller representation involves spectral measurements. Indeed, simply using RGB can lead to notorious problems in generating synthetic images [47]. Thus a more complete description of light spectra involves specifying quantum catches for narrowband filters (with widths of around 10nm), at least over the spectral sensitivity of the Human Visual System (HSV), which ranges from 390 to 750nm. Since light is an electromagnetic wave (macroscopically), one might wonder whether the Spectral Power Distribution (SPD) thus obtained is indeed sufficient for describing image formation for Graphics or for Computer Vision, but in fact it can be shown that the SPD is sufficient [76]. In this thesis, data available is typically inclusive of, but well beyond the spectral range of the HSV.

1.1.2 Surface Reflectance

In physics surface reflection is the change in intensity and direction of an incoming light ray, in the case of geometrical optics, between two different media so that the light ray returns into the medium which it comes from. Reflection of light can be specular or diffuse. Perfect specular reflection from a surface is mirror-like, in which the incoming light ray is emitted into a single direction. This reflectance is based on the geometry of the surface and can be described by the law of reflection. The law of reflection states that incoming and outgoing light rays and surface normal are co-planar, and the angle between incident ray and surface normal is equal to the angle between reflectance ray and surface normal.

Diffuse reflection is a reflection from a surface where the incoming light ray is reflected in many angles, unlike perfect specular reflectance where it is reflected into a single angle. If the reflected luminance is equal in all directions, then the surface is called Lambertian, and the surface reflectance can be described by Lambert's cosine law: the shading is given by the cosine of the angle between the incoming ray and the local surface normal (and clipped to zero for normals at greater than 90° from the light direction). In general in Nature, surface reflectance consist of both specular and diffuse reflectances. A simplified model for combining both is the Dichromatic Reflection model [51], which holds in the spectral domain as well as in RGB. This states that, for a single surface, the spectrum lies in a plane formed by the diffuse spectrum and the specular one. In Graphics, the Phong model for specular reflection [63] is often used, notwithstanding its simplicity: this uses a cosine of the angle between the surface normal and the viewing angle to generate a more spread-out specular reflectance cone. The Neutral Interface Model [55] goes on to propose that specular colour shall be equated with that of the light itself. This holds, approximately, for dielectrics (but not for

metals).

1.1.3 Colour

Since colour is 3-dimensional for the HVS, in that there are three types of colour sensors in the human eye [56], many different colour models have arisen for different purposes, each based on 3-vector descriptions. Some of these are RGB, XYZ, HSV, YUV, CIELAB, CIEXYZ, CMYK, etc. [56].

Here we are exclusively interested in (i) RGB values as seen by a camera and (ii) colour triples as seen by HVS. For the latter, "colour" is taken to be the triple formed by integrating the light-stimulus SPD with the human colour-matching functions [79], denoted $\bar{x}(\lambda)$, $\bar{y}(\lambda)$, $\bar{z}(\lambda)$. That is, a tristimulus 3-vector X, Y, Z is formed by

$$\begin{aligned} X &= \int E(\lambda)\, \bar{x}(\lambda)\, d\lambda \\ Y &= \int E(\lambda)\, \bar{y}(\lambda)\, d\lambda \\ Z &= \int E(\lambda)\, \bar{z}(\lambda)\, d\lambda \end{aligned} \tag{1.1}$$

where $E(\lambda)$ is the light SPD entering the eye. The middle value, Y, is called the *luminance*.

For 3-dimensional colour image data, human vision sensors are replaced by camera sensors. Let us denote these three sensors, corresponding to R, G, B as spectral sensitivity curves $\boldsymbol{q}(\lambda)$, with components

$$\boldsymbol{q}(\lambda) = (q_R(\lambda), q_G(\lambda), q_B(\lambda))^T \tag{1.2}$$

Then for camera values R, G, B pixel values are generated in a similar manner to Equation (1.1), as follows:

$$\begin{aligned} R &= \int E(\lambda)\, q_R(\lambda)\, d\lambda \\ G &= \int E(\lambda)\, q_G(\lambda)\, d\lambda \\ B &= \int E(\lambda)\, q_B(\lambda)\, d\lambda \end{aligned} \tag{1.3}$$

1.2 Illumination Effects

Illumination effects are well studied in both optics and in the computer graphics. Illumination has many effects on the perceived image by HVS or computer. It is important that a computer-generated image be perceived as *"real"* by humans. It is also important that a human made scene

be perceived as *"understandable"* by a computer. Illumination plays a big role in both perceptions. Factors such as intensity of the illumination and its colour has effects on the perceived image, in addition to shading and specularity, which come from geometry of single object in the scene and illumination direction, and last but not least shadows have great effects on perceived shape and colour of the objects in a scene.

By definition, illumination intensity is the amount of light that hits or passes through a unit surface. In photometry intensity is measured as the amount of light perceived by human eye, and is measured in Lux, the standard unit for luminous power per unit area. Intensity of illumination source may vary by the wavelength of light, but the perceived brightness by human eye is related to the total amount of intensities over all the visible wavelengths.

Shading is another important effect of illumination which is caused by the geometry of the object. In a brief explanation, shading is a change in brightness caused by change in angle between the surface normal vector and illumination rays. This effect is very important in computer graphics for rendering realistic images. Usually images without shading seem to be flat for humans. That is the reason that shading is a huge contributor to perception of depth by humans.

Specularity or highlight is another important effect of illumination caused by the geometry of the object. For this specific effect not only surface normal vector and illumination rays are important, but also the viewer's direction. Usually a specular point is perceived as a point which returns all the incident light rays to the viewer—like a mirror. Based on this effect different materials are divided into two groups: one is matte materials which do not have any specularities, and another is specular materials which may have specular points.

Figure 1.2 shows shading and specularity for a sphere. Please note that the image is not real, it is synthesized based on Phong's model of reflection.

Figure 1.2: Shading and Specularity for a Sphere

Another important effect of illumination is shadow. Shadow can be defined as lack of illumination caused by an obstacle, preventing illumination rays to reach a surface, resulting in darker surface reflectance in general. If some part of the object was the obstacle, then the shadow is called

self-shadow, while it is called cast shadow otherwise.

1.3 Previous Works

As mentioned earlier regarding the effect of illumination on images and the problems that different illumination conditions can cause for tasks like segmentation, detection and recognition, it is very important to be able to separate changes in image surfaces from changes in illumination conditions. This task is one of the fundamental tasks in computer vision systems due to its great influence on results. Due to the well understood importance of this issue, studies on separating illumination effects from reflectance have appeared for some time. Barrow and Tenenbaum [4] introduced *"intrinsic images"* in 1978 as a representation for decomposing reflectance variations from illumination variations. In their work intrinsic images are introduced as mid-level image descriptors which decompose the input image into two images, one which records surface reflectance for different points in the scene and another that records the variation of illumination across the image. Barrow and Tenenbaum proposed methods that can work under simple models of image formation. But since image formation is complex in nature recovering intrinsic images from an image is an ill-posed problem and cannot be solved without further limitations and conditions on the image. More recently Weiss [78] proposed a new algorithm for deriving intrinsic images from a sequence of images captured with a stationary camera. Instead of dealing with the general problem, Weiss assumed that the reflectance image will not change in the sequence of T images. He also assumed that the illumination image will give rise to sparse filter outputs. With these assumptions the problem became well-posed but the application of this method is restricted.

Another similar attempt to solve the problem of decomposing reflectance and illumination images from the input image is the Lightness and Retinex algorithms, first introduced by Land and McCann [54]. They have tried to decompose the input images into Lightness and Retinex images, which are reflectance and illumination images in intrinsic image decomposition, under certain conditions applied to the scene and illumination. They assumed that reflectance images will be piecewise constant and surfaces are 2-dimensional planar. They also use the assumption that illumination intensity will change slowly across the image. Under these assumptions they have distinguished changes in reflectance images and changes in illumination images. The method was extended over the years: works done by Horn [38], Hurlbert [40], Funt et al.[27] and Freeman and Viola [26] are good examples of those extensions, yet some limitations still restrict applications of this approach.

Attempts have not been limited to decomposing an input image into two images representing the surface reflectance and illumination intensity of the scene. Other approaches have taken the

colour of scene illuminant into account as well. Land's *"Retinex Theory of Color Vision"* [53] was seminal in an approach called Colour Constancy, where instead of obtaining the intrinsic reflectance images the objective is to obtain a rendering for a scene under different illumination. Colour constancy algorithms have been continuously improved over the years and works done by Maloney and Wandell [59], Forsyth [24] and Finlayson et al. [21] are examples of this research. These algorithms have often assumed the same restrictive conditions that lightness and retinex theory do, such a Mondrian scenes, which limits their applicability in natural scene conditions. Also, factors such as shadows, shading and specularities are often ignored.

Colour constancy algorithms try to estimate the colour of scene illuminant, but another approach is to *remove* its effects from images instead of estimating it. The work done by Funt and Finlayson [28] is based on that intuition, using some invariant features which remain the same under different illumination conditions. They have proposed a new method to be used in color indexing instead of using colour constancy as preprocessing. They used the fact that ratios of colour RGB values for neighbouring locations are almost invariant with respect to illumination of the scene. There are other methods using a similar intuition, such as works by Healey and Wang [36], Gevers and Smeulders [30] , Gevers and Stokman [31] and Finlayson et al. [14].

The next group of methods concerned with illumination effects on images are methods dealing with both intensity and colour of illuminant that form so-called shadow-free algorithms or in a more general sense illumination-free algorithms. 3-dimensional colour constancy algorithms, in the RGB domain, are too difficult to solve as proposed in [54, 59]. If we move to the chromaticity domain, which is 2-dimensional, the problem of colour constancy is more tractable, as in [22]. Finlayson and Hordley proposed a new method in [19] where they address the 1-dimensional colour constancy problem under certain assumptions. Here the objective was to simply derive a greyscale (1-D) image which is invariant with respect to lighting change. They have shown that 1-dimensional colour constancy is same as invariant computation at a pixel. Their method was the basis for some successful extension of shadow-free methods such as works done by Finlayson and Drew [15], Finlayson et al. [20] [17] [23], Drew and Finlayson [9] and Drew and Yazdani Salekdeh [10].

Although general illumination effects have been well studied in the above-mentioned works, there are a number of works which deal with specific effects of illumination, such as shadows. Shadow formation is one of the well-studied effects of illumination and shadows have significant influence on different computer vision algorithms. Due to its influence, there are numerous vision systems that deal with shadows to reach better results. Methods proposed by Salvador et al. [68] [69] are based on invariant colour models to identify and classify shadows [68] and to segment cast shadows [69]. In the first method they divide shadows into two classes, cast shadows and self shadows, but in the later work they add dark objects as a classification class as well. They

first find the candidate regions for shadows based on the assumption that shadows are darker than non-shadows. In the next step they try to classify candidates based on invariant colour features when assuming that ambient light is proportional to the direct occluded light. Their method is very similar to the method proposed by Javad and Shah in [44]. There are other attempts to solve the problem of detecting cast shadows in videos such as Stuader et al. [72] and Jacques et al. [41] but still all those algorithms only try to detect the shadow, and remove it from the calculations in the vision task, not remove effects of shadows in the images.

Another field that shows interest to deal with shadows is Human-Computer Interaction. User-cast shadows are not desirable in interactive displays, but this situation happens frequently in front-projector displays. Using back-projecting displays are limited in HCI since they need a special display surface material but the front-projector displays are easy to handle and more affordable. This is the motivation behind the work of Sukhtankar et al. [75] and Jaynes et al. [46] [45] who use multiple projectors and cameras to find the shadow region and relight it using redundant projectors. Although their work is not related to other methods mentioned in this chapter, it shows the importance of illumination effects in different fields of computer science.

The above mentioned methods deal with illumination effects, however most of them only work in 3-dimensional colour space and are not designed for multispectral and hyperspectral image data. Dealing with satellite and aerial image data has a strong background in Geoscience and Remote sensing community, and the early works in that community pay special attentions to illumination effects in multispectral and hyperspectral images. Ranson and Daughetry's work [64] on Scene Shadow Effects is one of the earliest works, which studied effects of strength and position of shadows on multispectral responses from vegetation surface. They have used 7 channels image data with 3 channels in the visible domain and 4 others beyond visibility and shown that the multispectral response is greatly influenced by shadows in the scene. They also mentioned that shadows can affect classification results for vegetation classification, which has been studied by Franklin et al. in [25] and by Singh and Cracknell in [71] as well.

Approaches for finding and removing the shadow areas in hyperspectral images were studied later in [35] and [1]. More recently, Adler-Golden et al. [2] proposed a method to removing shadows from spectral imagery. Their method first tries to find shadow "cores" by assigning a number to each pixel representing the proportion of shadow for that point and finding the maximum assigned numbers. In the next step they find the shadows by expanding those shadow cores and after finding the shadowed region they try to amplify the spectrum for those points. A similar approach has been used by Richter in [66]. His proposed method has special requirements about wavelengths of the sensor, which has been used in finding the shadow cores. After that a region growing approach is used to find the shadowed area and de-shadowing is done using scaled shadow functions.

Montoliu et al. in [62] proposed an invariant representation to intensity, highlights and shading for multispectral images. They have used dichromatic reflection model as physical model, and based on assumption that the illumination is perfect white, removed the illumination effects by L_n Multispectral Invariant method. Although their results showed effectiveness of their method, the assumptions they have made in their method are not applicable to real world images. The same assumptions have been used by Stokman and Gevers in [73] where they detect and classify hyperspectral edges. They put edges caused by material changes, surface orientation and shadows in different classes and used hyperspectral information to distinguish between them.

Recently another method for suppressing illumination effects has been proposed by Ashton et al. in [3]. In their method they convert data from Cartesian space to hyperspherical coordinate system, then segment the data into many classes using K-means and after that subtract the mean from each class to remove shadows. They compare their method to normalize magnitude methods and state that normalize magnitude methods will not work for shadows.

Spectral images have been used in other applications as well. For example Suen and Healey used hyperspectral imagery for recognizing faces invariant to illumination [74], Ye et al. have used spectral and shape priors to segment aerial hyperspectral images from airplanes [81] and Brown and Susstrunk have used multispectral SIFT features to improve performance in scene recognition.

Many channels in hyperspectral images and the diversity of those channels, from visible to far beyond visibility, made it hard to visualize the hyperspectral images. There are methods proposed for visualizing the whole spectrum of hyperspectral images in past decades. Since all images that we display on our day to day displays such as CRT, LCD and TV, have 3 components such as RGB, HSV, etc. the question is how to reduce that many channels to three, to be able to visualize them on displays.

One standard answer would be using dimension reduction approaches such as Principle Component Analysis. Using PCA, one can choose the first three components images, which represent the maximum data variance, and use them as RGB or HSV values. This approach has been used in works by Ready and Wintz [65], Tyo et al. [77] and with some changes using wavelets by Gupta and Jacobson [32]. Although this approach is simple and will result in a colourful images, since the basis will change for different images the resulting visualized images are not interpretable or comparable.

Another approach to visualize hyperspectral images is to use a mega pixel. This approach has intuitions in the fact that in hyperspectral images, each pixel does not correspond to a single material type. Sometimes a pixel in the image represents different amounts of various materials, which is important in remote sensing and there are many methods to determine the materials and their proportion in each pixel. Based on these facts an approach proposed for visualizing

hyperspectral images is to have a mega pixel, and based on materials in each pixel, assign different colours, textures, etc. to that pixel. This approach has been used by Erbacher et al. [13], Healey and Enns [35], Cai et al. [6] and Du et al. [12].

Cai et al. [6] have used a fan like mega pixel and 6 classes. Each mega pixel can have different proportions of each colour based on the proportion of the material that colour represents. They used Red, Green and Blue and in addition to them they have used Yellow, Sky Blue and Purple to represent materials. Although this approach is based on intuitions that come from the context of remote sensing, since it needs classification as preprocessing for visualization, it is hard to implement and time consuming. Du et al. [12] extend [6] by trying to display all useful information in the visualization and try to make the visualization as distinctive as possible.

In another attempt to solve the problem, Jacobson and Gupta in [42] proposed a method to show hyperspectral images on tristimulus displays using spectral envelopes. They have aimed to create a natural-looking representation of hyperspectral images where white points, brightness, saturation and hue have the same meanings as they have in the human visual system. Their method was inspired by the human visual system. They tried to generate spectral envelopes that use whole spectral domain to generate 3 sensor values. They tried different envelopes such as stretched CIE Colour Matching Functions.Their method is simpler than using mega pixels yet unlike PCA which is adaptive to different images it is fixed for all images and thus interpretable. Jacobson et al. extended this work in [43] by using various envelopes and showed other applications of visualizing hyperspectral images such as radar images. They also have shown effectiveness of their method for classification.

Chapter 2

Spectral Images

In order to build a system which can remove effects of illumination in images, we first should study how images are formed. This study not only will give us intuition on potential solutions to our problem, but also will give us a broader view of the problem which will help us with analysis of outputs to refine our models or find why some method works while the other does not.

With this regard, the chapter started with image formation equations and formulas for multispectral and hyperspectral images. Although they are closely related together, there are some small differences and issues are worth mentioning.

2.1 Multispectral Image Formation

To begin with, let us briefly state the model we adopt for multispectral image formation.

Let $\boldsymbol{\rho}$ be a 31-vector for wavelength λ=400 to 700nm at 10nm intervals, determined by sampling scene spectra using a narrowband spectrophotometer such as the PhotoResearch PR-650 or the SpectraCube [29].

Let us assume that the scene illuminant is constant across the scene, and is given by Planck's Law [79]:

$$P(\lambda) \;=\; c_1\,\lambda^{-5}\left[\exp\left(\frac{c_2}{T\lambda}\right)-1\right]^{-1} \tag{2.1}$$

This equation is simplified in Wien's approximation:

$$P(\lambda) \;=\; c_1\,\lambda^{-5}\exp\left(-\frac{c_2}{T\lambda}\right) \tag{2.2}$$

with constants c_1 and c_2, where temperature T characterizes the lighting colour. Specifically, $c_1 = 3.74183\times10^{16}$; $c_2 = 1.4388\times10^{-2}$ (note that for these units, λ is in meters).

Let a multiplicative shading term at a pixel be denoted σ (and this could be Lambertian shading — normal vector dotted into normalized lighting direction).

We shall not make use of constant c_1 above, but instead use an overall multiplicative light intensity scalar I. As well, let us denote by $S(\lambda)$ the surface spectral reflectance function.

For completeness, we address not only matte reflectance but also a possible specular contribution, in a spectral image formation model. Suppose the strength of a specular term is given by scalar β. If we adopt the Neutral Interface Model [55], here moved into the spectral domain, the spectrum for the specular part of the light reflected from a dielectric is simply given by that of the light itself.

Finally, assuming that our spectrophotometer is sufficiently narrowband, then each sensor is effectively a delta-function, filtering out all wavelengths except λ_k, for the peak wavelength of the kth sensor. Since the measuring instrument may in fact provide different gain factors in each spectral channel $k = 1..31$, we should also include in our model an unknown (although in principle measurable) 31-vector q_k representing the measurement gain in each channel. [Note: We do not need to measure or know this vector, for this work.]

Hence, overall, we model the multispectral signal as:

$$\rho_k \;=\; \sigma I \frac{1}{\lambda_k^5} \exp\left(-\frac{c_2}{\lambda_k T}\right) S(\lambda_k) q_k \;+\; \beta I \frac{1}{\lambda_k^5} \exp\left(-\frac{c_2}{\lambda_k T}\right) q_k \tag{2.3}$$

Combining both terms, and defining $\alpha \equiv \beta/\sigma$, we thus have an exponential light-colour term times a factor

$$\sigma I \left[S(\lambda_k) \;+\; \alpha\right]$$

and thus we would have

$$\rho_k \;=\; \sigma I \left[S(\lambda_k) \;+\; \alpha\right] \left(\frac{1}{\lambda_k^5} \exp\left(-\frac{c_2}{\lambda_k T}\right) q_k\right) \tag{2.4}$$

as our final image formation formula.

2.2 Hyperspectral Image Formation

Hyperspectral image formation is very similar to multispectral image formation in its nature, in the sense that both are spectral images with narrowband sensors. Each sensor has a gain and a peak wavelength. Using these similarities we can say that image formation formulae for hyperspectral images and multispectral image formation formulae are the same. In fact that is true but still there are differences between multispectral and hyperspectal images which we have to pay attention to. These differences are in the number of channels and the domain of the channels.

One important issue with hyperspectral images is number of channels. Most hyperspectral images are from satellite or aerial imaging devices. Sending a satellite to space or flying special airplanes for aerial imaging are so expensive that the price of most accurate cameras with widest range of sensor wavelength is negligible. Due to this fact, recorded hyperspectral images have many channels, usually more than 200. This number could be even more than 350 channels in some cases. The size of data is directly proportional to the number of channels, so in working with hyperspectral images the data size is about 10 times greater than when working with multispectral images. This can make it more difficult for computer vision algorithms to work on hyperspectral images efficiently, and in timely manner.

The domain of channels in multispectral and hyperspectral images are different. Usually many channels in hyperspectral images are beyond visibility range of human beings. This makes it different from multispectral images where all the channels are between 400 to 700 nanometers - visible domain of humans. This difference not only makes it difficult to show input images but also makes it more difficult to interpret the results and to show effectiveness of the methods in removing effects of illumination. Not paying enough attention to this difference can cause false interpretations of resulted images.

After mentioning these differences and with regards to similarities between hyperspectral and multispectral images, we can use Equation 2.4 which is final image formation formula for multispectral images, and also for hyperspectral images. The only difference is that for hyperspectral images $k = 1..N$ where $N = 224$ or $N = 360$ for datasets used in this work.

2.3 Removing Illumination Effects - Problem Definition

While RGB colour is useful in recognizing or identifying objects and surfaces, it is of course dependent on the illumination incident on the surface. This dependency is not desirable and in most cases can increase error rates and decrease accuracy of the results in computer vision tasks. This has led researchers to develop a number of features that are to some extent *invariant* to the colour or intensity of the illuminant, and to shading as well if possible. Most of these invariant features use information from all pixels in the image in their construction. For example, suppose we normalize an image by dividing Red by its mean value, and similarly for Green and Blue: it can be proved that under certain assumptions this will indeed remove the effect of lighting [11], and if we go over to a chromaticity representation – colour without magnitude – then we can to some extent remove shading as well and arrive at surface colours that provide an intrinsic property of the object itself rather than depending on the sensor and the conditions under which the object is viewed.

Recently, however, a new type of invariant has been constructed that works using only the

information at each pixel [19]. To generate this invariant, sensor (camera RGB) information is required in the form of a set of calibration images, taken under different illumination conditions [20]. One important benefit of the invariant is that since illumination is effectively removed, so are shadows. But for a non-laboratory setting, calibration images are not available and instead entropy information taken from a single image can be used to develop the parameters necessary to produce an invariant image [18]. Nonetheless, generating an invariant image remains a complex and error-prone task for RGB image data.

Using multispectral or hyperspectral image capture, instead of coarsely sampling scene information using broadband camera sensors, samples the signal much more finely. The utility of this information is the possibility of spectral reconstruction of an entire scene and consequently more accurate reproduction and other uses such as identification of surface materials. This application of multispectral and hyperspectral data is studied thoroughly in remote sensing and geology. In terms of photometric-invariant image formation, for hyperspectral or multispectral data, although the amount of data is increased substantially the situation is in essence greatly simplified: one of the requirements for forming a strong invariant is the necessity of either making use of a narrowband-sensor camera or of generating an approximately narrowband set of sensors [16]. In this work, we usually indeed already have narrowband multispectral and hyperspectral sensors, and also know the peak wavelength for each of these. This situation simplifies the generation of an invariant and we show that with this simple knowledge of peak wavelengths we can generate multispectral and hyperspectral data from the input such that the algorithm output is to a great degree invariant to illumination colour and strength, and has shading removed. In fact, the invariant produced is a good deal more effective in removing the effects of shading and lighting because of the greatly increased information available compared to 3-camera-sensor images.

In this work the problem to be solved is to remove the effects of illuminations in multispectral and hyperspectral images, in the situation that we know the peak wavelengths. The effects consist of shading, shadows, colour and intensity of illuminant, inter-reflection and specularities. In § 4 the results are shown.

Chapter 3

Method

In §2 the image formation process for spectral images was discussed and the differences between hyperspectral and multispectral images have been mentioned. Furthermore, the reasons that these effects are not desirable in various applications of multispectral and hyperspectral images have been discussed and the problem of removing illumination effects has been defined. In this chapter the new method for removing illumination effects for spectral images is proposed and explained in detail. In the first section, the method for multispectral images is explained, and in the second section different versions of the method for hyperspectral images are discussed. Results can be find in §4 for synthetic and measured multispectral images and measured hyperspectral images on different image data. More discussions and conclusion will be in §5.

3.1 Multispectral Images

As shown in in § 2.1 we model the spectral signal of k^{th} channel as Equation 2.3 where $k = 1..31$. By combining both terms, and defining variable $\alpha \equiv \beta/\sigma$, we have an exponential light-colour term times a factor

$$\sigma I \left[S(\lambda_k) \, + \, \alpha \right]$$

From there we came to our final multispectral signal formation formula which has been shown in Equation 2.4.

Since light intensity I and shading σ are scalars in Equation 2.4, we can derive a signal which is invariant to light intensity and shading by dividing values for every signal channel k by one particular value of one of the 31 channels. This normalization-like process will form a chromaticity as in [19]. Dividing by one particular channel is common when we know the application. Mouth and lips localization and in general face detection using skin colour are examples of that (cf. [39]). In general, however, in order to not place undue confidence in any particular channel using

arithmetic mean in denominator is preferred as in [80] and [50]. In our work instead, we divide by the geometric mean of the $\boldsymbol{\rho}$ values (cf. [15]). This way we not only remove confidence on one particular channel, but we also use properties of the geometric mean when applying log function to form log chromaticities.

Let us define a chromaticity χ_k as dividing by the geometric mean value

$$\rho_M \equiv \left(\prod_{j=1}^{31} \rho_j\right)^{(1/31)} \tag{3.1}$$

so that we generate a modified type of band-ratio chromaticity (colour without magnitude) via

$$\chi_k = \rho_k/\rho_M, \quad k = 1..31 \tag{3.2}$$

This is a modified type of band-ratio chromaticity since the normal chromaticity is formed when channels are divided by arithmetic mean (usually in 3D colour space like RGB). In that case sum of all chromaticity values will be equal to 1. Here in this modified version of band-ratio chromaticity, instead of summation the multiplication of chromaticity values will be constant equal to 1. This means that the log of chromaticity space is a subspace perpendicular to vector $(1, 1, 1)$ - in 31-dimensional case to 31-dimensional vector $(1, 1, ..., 1)$.

Substituting our signal formation model Equation 2.3 in chromaticity equation, we arrive at the form

$$\chi_k = \left(\frac{S(\lambda_k)+\alpha}{S(\lambda_M)+\alpha}\right)\frac{\lambda_M^5}{\lambda_k^5}\ \exp\left(-\frac{c_2}{T}\left[\frac{1}{\lambda_k} - \frac{1}{\lambda_M}\right]\right)\frac{q_k}{q_M} \tag{3.3}$$

or

$$\chi_k = \left(\frac{s_k+\alpha}{s_M+\alpha}\right) w_k\ \exp\left(\frac{1}{T}\left[e_k - e_M\right]\right)\phi_k \tag{3.4}$$

where we simplify the expressions by defining some short-hand notations as follows:

$$v_k = \lambda_k^{-5};\ w_k = v_k/v_M;\ \phi_k = q_k/q_M;\ s_k = S(\lambda_k);$$

$$e_k = -c_2/\lambda_k;\ v_M = \left\{\prod_{j=1}^{31} v_j\right\}^{1/31}; \tag{3.5}$$

$$q_M = \left\{\prod_{j=1}^{31} q_j\right\}^{1/31};\ e_M = (1/31)\sum_{j=1}^{31} e_j$$

and we define an effective geometric-mean-respecting value s_M by setting

$$(s_M+\alpha) \equiv \left[\prod_{j=1}^{31}(s_j+\alpha)\right]^{1/31}$$

The light-colour information as in Equation 2.1 and Equation 2.2 is controlled by temperature T, and it is contained in an exponential. It makes sense to take logarithms to remove exponentials

and change multiplications to summation. Then rewriting, the log of the chromaticity now becomes

$$\log \chi_k \;=\; \log\left(\frac{s_k+\alpha}{s_M+\alpha}\right) \;+\; \log w_k \;+\; \log \phi_k \;+\; \frac{1}{T}(e_k - e_M) \tag{3.6}$$

Of course, any version of a chromaticity is meant to hold "colour" information with magnitude normalized away, and hence chromaticity signal values are not independent. Specifically, here the log values above all inhabit a plane orthogonal to the unit vector $(1,1,...,1)/\frac{1}{\sqrt{31}}$ in 31-dimensional space. And in fact each separate term in Equation (3.6) is orthogonal to that unit vector.

This means that although log chromaticity values are still 31-dimensional vectors, they are indeed live in 30-dimensional space. The reason that we still got 31-dimensional vectors is that instead of dividing by one of the channels which would lead us to 31-dimensional space with value one for that specific channel and thus a 30-dimensional space by removing that channel, we divide by geometric mean and now our plane is not orthogonal to any specific channel but instead to geometric mean of all channels.

So far we have removed intensity I and shading σ by forming chromaticity. Now we have to remove the effect of light colour. The only parameter determining light colour in our equation is T and in Equation 3.6 we can see that it's multiplied by vector $(e_k - e_M)$. This means that in order to remove the effect of light colour, we need to project the spectral information into a subspace orthogonal to the direction of the lighting term $(e_k - e_M)$. This projection will remove the term $\frac{1}{T}(e_k - e_M)$ from log chromaticity equation and thus remove effects of light colour.

Previously, in RGB space [19], we had to calibrate a camera system in order to recover this lighting direction; alternatively we could make use of the lighting-change information in an image to use an entropy measure to determine this direction [17]. But here, in the multispectral domain, we have a very special situation in that every signal channel is narrowband and is assumed given on specific, known wavelengths.

It worth mentioning that sensors were assumed to be narrowband in previous works like [19] and [17], but in our case working with spectral data made it possible for us to use narrow band sensors as a fact and not an assumption. We have used this fact in our equations and methods. Consequently we already know the special direction $(e_k - e_M)$ orthogonal to which to project in order to remove light colour information: $(e_k - e_M)$ is simply given by $(-c_2/\lambda_k - c_2/\lambda_M)$ and is known.

Also, the term $\log w_k$ in Equation 3.6 is also already known, for the same reason and we can compute it once we know the wavelengths of our narrowband sensors. Hence the only unknown sensor term in Equation 3.6 is the term in sensor gains, $\log \phi_k$.

As mentioned in §2.1 we have adopted Neutral Interface Model in our image formation equations. Using that we could in fact also derive the value of a projection of this sensor-gain 31-vector $\log \phi_k$

provided we could correctly identify at least one specularity in the image. For that specular point if we had a pure specularity (i.e., the same as imaging the lighting itself), the first term in Equation 3.6 goes to the zero 31-vector, as the specular-strength value α becomes large. So in fact at such a specularity, using the known other terms, we could determine the projected part of the $\log \phi_k$ vector, pertaining to the geometric-mean-divided gain chromaticity vector q_k/q_M.

This could have simplified our task a lot where with finding one specular point we could have known all the unknowns in our Equation 3.6. This could have been the case if the neutral-interface model we have adopted worked perfectly. However we found in practice that specular multispectral 31-vectors in a multispectral image are not, in fact, sufficiently free of surface reflectance effects from s_k to allow correct identification of the specular point. Therefore we must rest content with obtaining all terms except $\log \phi_k$ in Equation 3.6 (barring discovering this term via a calibration). Nonetheless, we can still obtain a multispectral illumination invariant without knowing the term $\log \phi_k$. In fact the term $\log \phi_k$ will become our origin in invariant space.

We have removed the effect of light intensity and shading by going over to a chromaticity space (thus basically descending from a 31-dimensional space to a 30-dimensional one, since chromaticity components χ_k are not independent but live on a 30-dimensional plane). To remove the effect of lighting colour, encapsulated in temperature T in Equation 3.6, we can project the data, written as 31-dimensional values, into a subspace orthogonal to the lighting-change direction $(e_k - e_M)$.

For suppose the (31×31) projection matrix which would be symmetric, idempotent, with a single non-zero eigenvalue, in light-change direction $(e_k - e_M)$ is given by matrix P_e. Then we can remove the effect of temperature T by pre-multiplying log chromaticities (Equation 3.6) by the projector onto the orthogonal subspace, $P_e^\perp = I_{31} - P_e$, where I_{31} is the 31×31 identity matrix.

Thus we obtain

$$P_e^\perp \log \chi_k \;=\; P_e^\perp \log \left(\frac{s_k + \alpha}{s_M + \alpha} \right) \;+\; P_e^\perp \log w_k \;+\; P_e^\perp \log \phi_k \tag{3.7}$$

We know the second term on the right because we know the narrowband signal wavelengths being measured. At a specularity, the first term on the right approximately vanishes — this is because the specular-factor term α dominates the surface-reflectance terms. At a non-specular pixel, the first term on the right is the matte characteristic of the surface material itself, and thus forms an illumination invariant.

We take the left hand side of Equation 3.7 to define our illumination-invariant multispectral image. In the following, we shall no longer consider the specular term for multispectral images but instead concentrate on matte components of images. You can find the Psuedocode for the multispectral illumination invariant algorithm in Program 3.1

```
Output = Multispectral_Invariant ( Spectral_Image )
{
        For each Pixel in Spectral_Image
                Geometric_Mean=Product(Channels)^(1/Count(Channels))
                Chromaticity = Pixel / Geometric_Mean
                LogChromaticity = Log(Chromaticity)
                Projector_e = Projector(e_k - e_M)
                Projector_Orthogonal = I-Projector_e
                ProjectedLogChromaticity = LogChromaticity * Projector_Orthogonal
                Output = Exp(ProjectedLogChromaticity)
        End
}
Visualize_Multispectral(Output)
```

Program 3.1: Psuedo-code for multispectral image invariant algorithm

We show below that this simple formulation works very well on real, 31-dimensional, multispectral data. To better understand the strengths and limitations of the model in Equation 3.7, first we consider multispectral synthetic images in §4.1, where we know the ground truth, and then in §4.2 go on to investigate experimental data.

3.2 Hyperspectral Images

As mentioned in §2.2, hyperspectral images are very similar to multispectral images in the sense that they both have narrowband sensors and the peak wavelengths for those sensors are known in spectral images. Also image formation formulas for both are the same. A question might come to mind; do we need a different method for removing the illumination effects from hyperspectral images? The answer is *"Yes and No"*.

Yes, in the sense that we are dealing with much greater data in terms of the size and number of channels, which needs a more efficient method to deal with, or an approach to reduce the size of channels before processing. Another issue would be the non-visible channels. As mentioned earlier, many hyperspectral channels are beyond visibility and need special attention when we are dealing with them. In fact only a small proportion of hyperspectral image data is in the visible domain. Not paying enough attention to non-visible channels can result in complications in visualizing the shadow-free image as well as the original image, and can cause false negatives and false positives.

On the other hand, the answer is *No* in the sense that with all differences between multispectral and hyperspectral images at the end they both are spectral images with the same image formation

formula. Since we do not have any assumptions about the number of channels or the visibility of those channels in our method presented in §3.1, then we can use the same method for hyperspectral images as well.

To conclude, both answers are correct and each of them addresses some issues about the defined problem as well as the proposed method. In this work we tested different versions of the method proposed for multispectral images with intuitions from the mentioned issues about hyperspectral images, and shown the differences and validity of those issues.

The first approach to solve the problem for hyperspectral images is to use multispectral illumination invariant method, by forming 31-dimensional data from the hyperspectral image data and then applying the exact method proposed in §3.1. This *"dimension reduction"* process can be done in many ways: choosing any 31 channels from our set of hundreds of channels, or choosing a specific set of channels, etc. Arbitrary choice of channels would prevent logical interpretation of the original and output image. Instead one can choose 31 sequential channels where all of those channels have peak wavelengths in the visible domain.

Another approach, which is used in this work, is to create an ideal 31-dimensional data using interpolation of hyperspectral image data. In this process we defined the ideal 31-dimensional image as an image where the peak wavelengths of its evenly spaced between 400 and 700 nanometers. We assumed that 400 to 700 nanometers is the human visible domain, however the lower and upper bands of the visibility domain varies in different sources.

Knowing the ideal peak wavelengths and the measured peak wavelengths of the hyperspectral image we can interpolate the ideal 31-dimensional image data using various interpolation methods. In this work we chose cubic spline interpolation.

Cubic spline interpolation, similar to other spline interpolations, is a piecewise polynomial interpolation. Spline interpolations are usually preferred over polynomial interpolation due to the ability of making interpolation errors small even using low degree polynomials. Using spline interpolation one can avoid the oscillation problem in interpolation as in Runge's phenomenon[67]. Runge's phenomenon occurs in interpolation with high degree polynomials.

For each piece, the cubic spline polynomial is formulated as:

$$P_i(x) = a_i(x - x_i)^3 + b_i(x - x_i)^2 + c_i(x - x_i) + d_i; x_i \leq x < x_{i+1} \tag{3.8}$$

for $i = 1..n - 1$ where n is number of data points, and a_i, b_i, c_i and d_i are coefficients of ith polynomial function P_i. Using some boundary conditions the equation above can be solved and coefficients can be determined [8].

Using cubic spline interpolation we can generate an ideal 31-dimensional version of the image data where information is in visible domain and we can apply the method proposed for multispectral

images and reach our output free from illumination effects. The psuedocode for this approach is shown in Program 3.2. However we had more information in the original input image which we threw away by making the ideal multispectral image. These information from the channels beyond visibility is useful in many applications and just throwing them away is not desirable for those applications.

```
Output = Hyperspectral_Invariant_1 ( Spectral_Image )
{
        Spectral_Image = Hyperspectral_To_Multispectral_Cubic_Spline( Spectral_Image )
        For each Pixel in Spectral_Image
                Geometric_Mean=Product(Channels)^(1/Count(Channels))
                Chromaticity = Pixel / Geometric_Mean
                LogChromaticity = Log(Chromaticity)
                Projector_e = Projector(e_k - e_M)
                Projector_Orthogonal = I-Projector_e
                ProjectedLogChromaticity = LogChromaticity * Projector_Orthogonal
                Output = Exp(ProjectedLogChromaticity)
        End
}
Visualize_Multispectral(Output)
```

Program 3.2: Psuedo-code for hyperspectral image invariant algorithm, the first approach — Using the cubic spline interpolation to reduce the hyperspectral input image into a multispectral image.

To solve this problem we can use the exact method proposed for making illumination invariant images in multispectral domain, to the hyperspectral image data and process all hyperspectral channels. This will need more computations and the problem can be hard to solve, but at the end we can be sure that we didn't throw out any information.

In order to visualize the input and output images we can use various approaches. One simple approach would be just visualizing the visible domain as we did previously. This will show the user what was the input image and what would be the output image if a person looked at it. This approach is simple and can show effectiveness of our algorithm in removing effects of illumination in visible domain, but the illumination has effects in beyond visibility domain as well. You can see the psuedo code for this approach in Program 3.3. It would not be fair to show the output of only visible domain when the algorithm uses the whole spectrum. On the other hand, the illumination effect might be still visually distinct for visible domains but not distinct taking all the channels into account. Based on these issues, we need to have some method to visualize the whole spectrum of the hyperspectral image.

an alternative is to use methods which allow visualization of whole hyperspectral spectrum for

```
Output = Hyperspectral_Invariant_2 ( Spectral_Image )
{
        For each Pixel in Spectral_Image
                Geometric_Mean=Product(Channels)^(1/Count(Channels))
                Chromaticity = Pixel / Geometric_Mean
                LogChromaticity = Log(Chromaticity)
                Projector_e = Projector(e_k - e_M)
                Projector_Orthogonal = I-Projector_e
                ProjectedLogChromaticity = LogChromaticity * Projector_Orthogonal
                ProjectedLogChromaticity = Hyperspectral_To_Multispectral_Cubic_Spline(ProjectedLogC
                Output = Exp(ProjectedLogChromaticity)
        End
}
Visualize_Multispectral(Output)
```

Program 3.3: Psuedo-code for hyperspectral image invariant algorithm, the second approach — Using the cubic spline interpolation to reduce the hyperspectral output image into a multispectral image.

each pixel. These methods have been mentioned in §1.3. Some of them use different envelopes to show the hyperspectral images the same way our eye sees the pictures in visible domain, while some others use mega pixels for each hyperspectral pixel. Using any of those methods can help visualizing the whole spectrum and prevent unfair judgments about the effectiveness of the method in removing illumination effects. Program 3.4 shows the psuedocode for this approach.

```
Output = Hyperspectral_Invariant_3 ( Spectral_Image )
{
        For each Pixel in Spectral_Image
                Geometric_Mean=Product(Channels)^(1/Count(Channels))
                Chromaticity = Pixel / Geometric_Mean
                LogChromaticity = Log(Chromaticity)
                Projector_e = Projector(e_k - e_M)
                Projector_Orthogonal = I-Projector_e
                ProjectedLogChromaticity = LogChromaticity * Projector_Orthogonal
                Output = Exp(ProjectedLogChromaticity)
        End
}
Visualize_Hyperspectral(Output)
```

Program 3.4: Psuedo-code for hyperspectral image invariant algorithm, the third approach — No dimension reduction

Although visualizing is a good solution, still it might be hard to implement or not satisfactory in every application. A simple alternative is to view the spectrum in plots. That way we can see the difference of spectrums of two points and compare the spectrums. This approach has been used for in-light and in-shadow points and shows the effectiveness of the method using them.

Chapter 4

Results

So far the problem is defined and the method for solving the problem is proposed. In this chapter results for synthetic and measured multispectral image data and measured hyperspectral image data from different imagery sources are shown.

4.1 Synthetic Multi Spectral Images

In order to check the validity of our method we first generate a simple synthetic scene, but using full spectra, so as to be able to completely control reflectances and illuminants in the spectral image. Such a synthetically generated 31-band image can then serve as a testing ground for our analysis, and can show that our method is working for the situation where all our assumptions are held.

Suppose we utilize a set of three shaded spheres as in [15], with surface colors equal to patches 1, 4, and 9 (dark skin, moderate olive green, moderate red) of the Macbeth ColorChecker [61]. As illuminant, suppose we take Planckian light, a blueish Planckian light with temperature $T = 10500°K$. For generating RGB images we utilize the set of three camera sensors for the Kodak DCS420 colour still camera, shown in Figure 4.1(a), and for the set of 31 spectral gain values q_k we use those shown in Figure 4.1(b) [these are taken to be simply the sum of the camera curves raised to a power].

Let the direction to the light be $\{0.5, 1.0, 3.0\}$, normalized. Then the matte image in a Lambertian model is as in top row of Figure 4.2(a), displayed in the sRGB (gamma-corrected) colour space [7] (note the effect of the very blue light and the blue-red mix in the ostensibly blue camera sensor). Note that we show images in RGB, but in fact the synthetic image is generated in 31-D. The Lambertian shading image is shown in the top of Figure 4.2(b).

Now since we mean to show that a 31-dimensional illumination invariant image is derivable via Equation (3.7), in the bottom row of Figure 4.2(a) we show the same three surfaces, but illuminated by a reddish Planckian light for temperature $T_2 = 2800°K$. Since we mean to demonstrate that

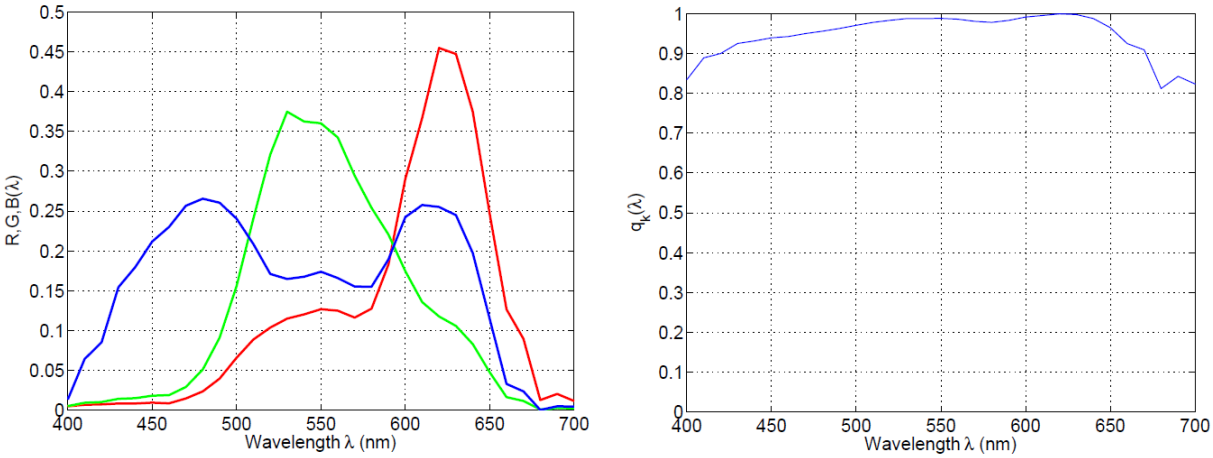

Figure 4.1: (a): Camera sensors; (b): 31-D sensor gains q_k

shading can be removed, in this case let the lighting direction be $\{-1.0, -2.0, 3.0\}$, normalized, so that shading is different than that for the blue light and is as in the bottom of Figure 4.2(b).

Now applying the invariant image formulation (3.7), we derive a 31-dimensional illumination invariant image. In terms of the geometric-mean chromaticity, we can display the resulting image, as in Figure 4.3.

/f

Here we have generated a colour image by applying the human vision colour-matching functions [79] to generate tristimulus XYZ values and then gone over to the standardized sRGB colour space.

To compare, in Figure 4.4, we show this chromaticity for the original, spectral, image, and note how differently the spheres appear under different lighting.

Since the invariant has in fact removed lighting, we show the chromaticity for the invariant regressed back onto that for the top of Figure 4.3 [as was done in [9] in order to put back some lighting]. Naturally, we cannot retrieve any information beyond the terminator for each of these sets of three spheres (where shading σ goes to zero).

Finally, we can ask how well we do in deriving a 31-dimensional invariant by calculating the mean Peak Signal-to-Noise Ratio (PSNR) for the spectral invariant, in the lighted (shading not zero) areas. PSNR is usually used as a measure of quality of reconstruction of compression methods which is related to similarity of the original and reconstructed image. PSNR is defined in Equation 4.1

$$PSNR = 20 \log_{10} \left(Max_I / \sqrt{\frac{1}{mn} \sum_{i=0}^{m-1} \sum_{j=0}^{n-1} [I(i,j) - O(i,j)]^2} \right) \tag{4.1}$$

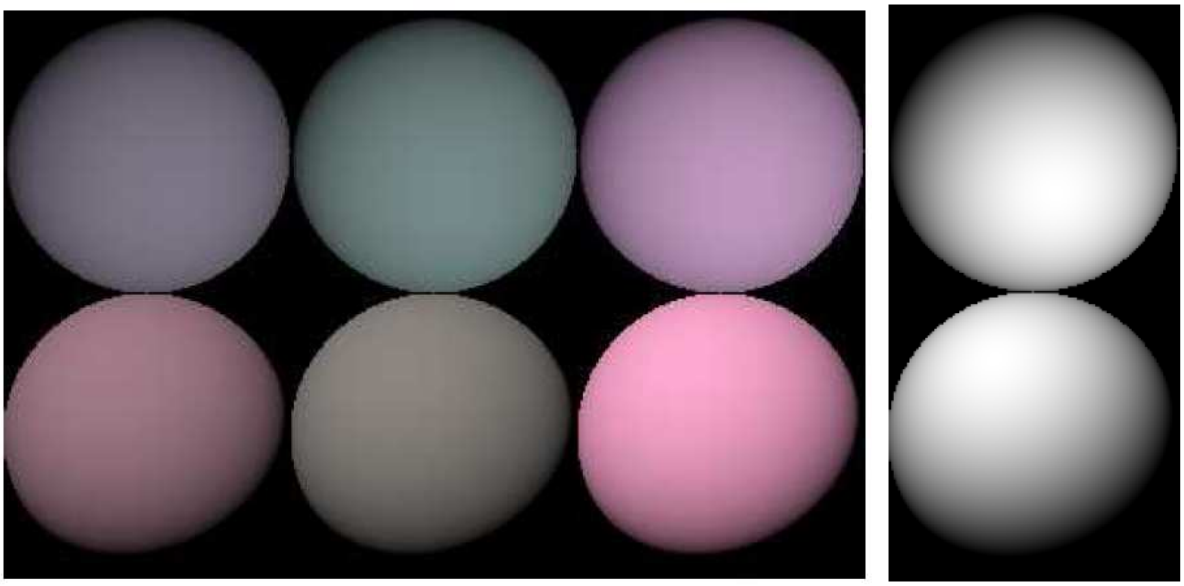

(a) (b)

Figure 4.2: (a): Matte image, top row under blue Planckian $T = 10500°K$, bottom under red $T = 2,800°K$; (b): Shading under each of two lights

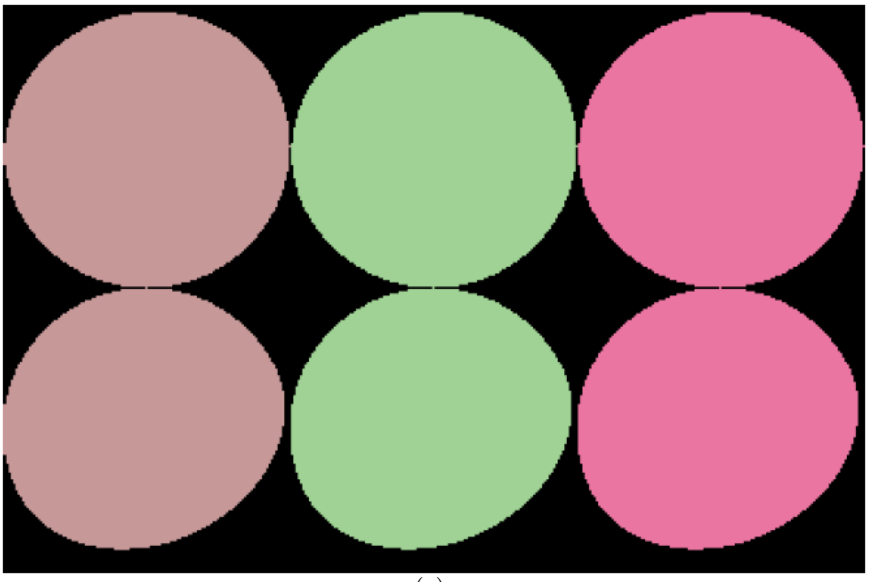

(a)

Figure 4.3: Illumination-invariant chromaticity image

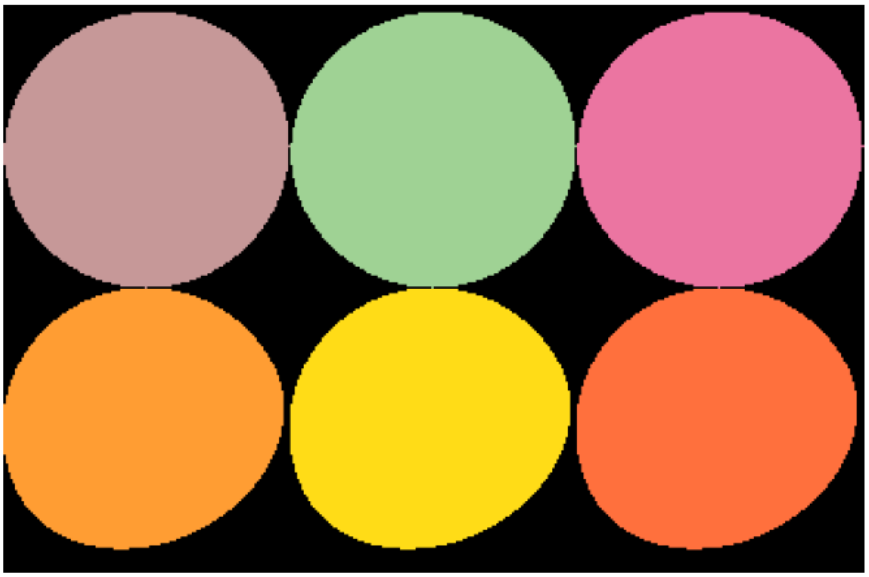

(a)

Figure 4.4: Chromaticity for original image before invariant processing

Where Max_I is the maximum value of the input image, I is the input image and O is the output image. We find a mean PSNR value of 73.87 dB for this synthetic example: since there is in fact so much data available, an illumination invariant (at least in this noise-free synthetic example) does better than typical results using only 3-sample RGB data (cf. Ref. [18]).

4.2 Measured Multispectral Images

To show our method's applicability to real multispectral images, let us apply the above analysis to measured multispectral image data: suppose that for visualization purposes we make RGB colour out of the spectral database image data collected in [37]. That is, we generate XYZ tristimulus values from the 31-D data by applying the human vision colour-matching functions and then go over to nonlinear (i.e., gamma-corrected) sRGB colour space pixel values by applying the XYZ to sRGB transformation in the sRGB standard [7].

Let us consider the 31-dimensional image visualized in Figure 4.5(a), displayed in sRGB colour space. This image is generated from 31-D spectral data imaged under standard daylight D75 [29].

Now, since we know the actual imaging daylight and in fact we have complete high-dimensional data, it is straightforward to *change the lighting* by dividing each spectral component by the light-vector value for the original illuminant, D75, and multiplying by a second light. Here we go over to a much more reddish-looking light, standard illuminant D48 [48], whose correlated colour

(a)

(b)

Figure 4.5: (a): Visualization of 31-D measured multispectral data, under illuminant D75 ; (b): Visualization under redder illuminant D48

temperature T is $4800°K$. Now the visualization appears as in Figure 4.5(b), i.e., with colours substantially shifted to the red.

Applying the invariant processing Equation (3.7), we derive illumination invariant 31-D multispectral images for each of the lights. Figures 4.6(a,b) show how the invariant appears in RGB, under each of the lights (where again we have regressed colours back onto those that do not have the lighting removed, Figure 4.5(a), as in [9]).

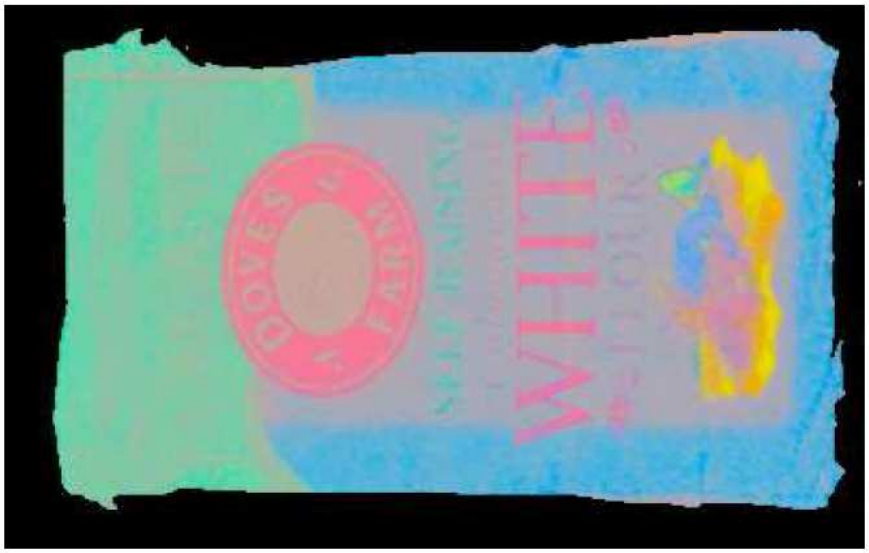

(a)

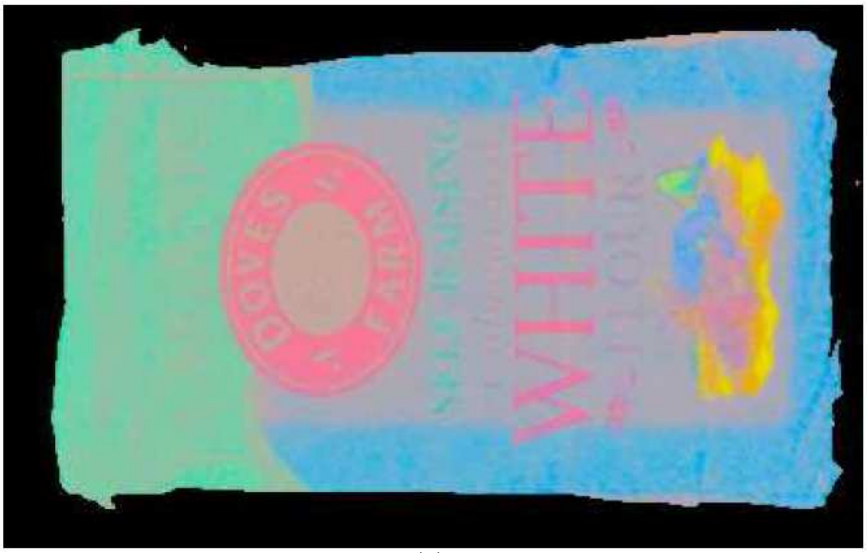

(b)

Figure 4.6: (a): Invariant derived from D75 image; (b): Invariant derived from D48 image

For the 31-dimensional invariant spectral images derived from each of the lights, we can calculate the PSNR between each of the 31-dimensional pixel spectra, between the two output invariant 31-dimensional images. Here, we find a mean value of 39.09 dB, showing that the invariant produced is excellent: changing the lighting does not greatly affect the invariant result.

We can further characterize the strength of the invariant by examining the error between the colour visualizations in Figures 4.6(a,b): we can ask how different is the perceived colour between Figure 4.6(a) and Figure 4.6(b) by applying the s-CIELAB colour-error metric [82]. Rather than

Figure 4.7: Two points, in-shadow (blue circle) and in-light (red circle)

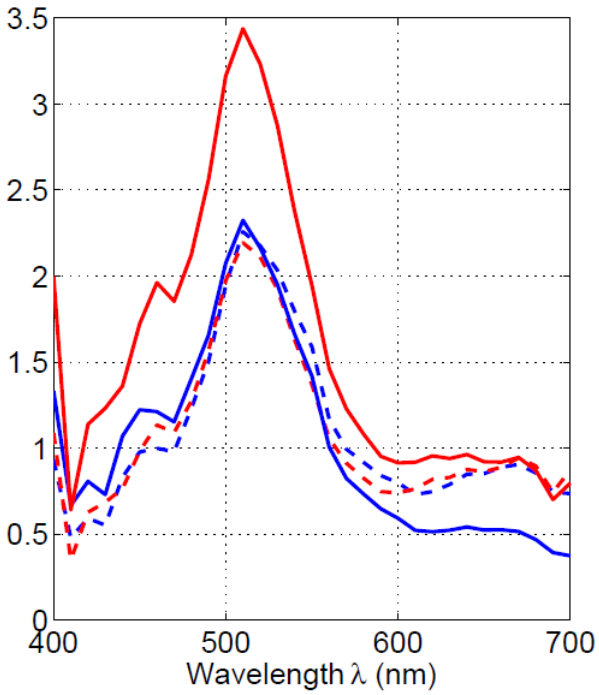

Figure 4.8: Plot of in-shadow (blue) and in-light (red) 31-D pixel data — solid curves are original data and dashed curves are after invariant processing

being simply a per-pixel error measure as is PSNR, this colour error metric takes into account human perception of colour difference including the effect of spatial visual acuity in the different opponent colour channels. Here, we find a very small colour difference, with maximum ΔE value 0.67, i.e., less than 1 just-noticeable difference value.

Figure 4.9: Multispectral Measured Images; Experiment results (Left: Original image; Right: Invariant)

While invariant images Figures 4.6(a,b) appear to retain somewhat the shadowing present in the original images, a close examination shows that this is not in fact the case: in the output images Figures 4.6(a,b) the shading inside locations that appeared in shadow is in fact correctly removed, and what now appears as shading is due to specularities that appear in the original data. Figure 4.7 identifies two points on the original image — the blue circle is in-shadow and the red

Figure 4.10: Multispectral Measured Images; Experiment results (continued) (Left: Original image; Right: Invariant)

one is in-light, both for the same surface material.

In Figure 4.8 the solid curves are for the original spectral data, blue for in-shadow and red for in-light. The dashed curves are for the corresponding invariant-spectral-image output — illuminant-invariant processing has brought the two curves into a much closer match, thus showing that that the 31-dimensional invariant does indeed substantially remove the effects of lighting and shading.

Figures 4.9 and 4.10 show both originals and invariant processing for a some of the further 19 images in the database used: the mean PSNR between invariant curves for all 20 spectral images under different lights varies from 37.78dB to 41.06dB, with mean value 39.34, showing that the multispectral invariant processing proposed here is very effective for removing lighting effects for this high-dimensional data. For colour error in RGB visualizations of the invariant between two standard lights, D75 and D48, the maximum spatial-CIELAB ΔE values range from 0.145 to 1.37 units, i.e. a very small perceptual difference.

4.3 Hyperspectral Images

4.3.1 SpecTIR Beltsville Dataset

As mentioned in §3.2 there are different approaches to remove illumination effects in hyperspectral image data. One is to reduce the data size to multispectral image with 31 channels and apply the method for removing the illumination effects in multispectral image data. For this we made the ideal 31 dimensional multispectral image from our hyperspectral image using cubic spline interpolation. To compare the invariant image with the original image we should reduce the original hyperspectral image into a multispectral image too.

The first dataset we used was SpecTIR Agriculture and Vegetation Sample from Beltsville, MD, USA[57]. The dataset has an hyperspectral image with 360 channels, with peak wavelengths from 390 to 2450 nanometers. The image has hight of 468 pixels and width of320 pixels. This dataset is one of the free sample datasets available on SpecTIR LLC. website.

In Figure 4.11(a) you can see RGB output of original hyperspectral image data of Beltsville using Kodak DCS420 camera sensors. In order to form the output we integrate data from all 31 channels to build RGB using the sensor gains as shown in Figure 4.1(a).

Since we have narrow band sensor responses, we can build the ideal output as shown in Figure 4.11(b) by choosing exact wavelengths of Red, Green and Blue equal to 610, 540 and 450 nanometers with sensor gains equal to 0.97, 0.69 and 0.50 respectively. This ideal delta function camera sensor response is shown in Figure 4.12. As you can see in Figure 4.11 output of the ideal delta function camera is sharper and seems nicer than output of Kodak DCS420, which is reasonable since the ideal camera should be more like a delta function camera and the bands should have less overlap possible.

We now can apply the same method developed for multispectral images as in §3.1. Figure 4.13(a) is the original image in chromaticity space. You can see the shadows as the strongest illumination effect on different parts of the image such as roads, parking lot, and in the forest.

Figure 4.13(b) show the result of our method in the chromaticity space. Since both images are

(a) (b)

Figure 4.11: (a) Kodak DCS420 camera Output (b) Ideal Delta function camera output

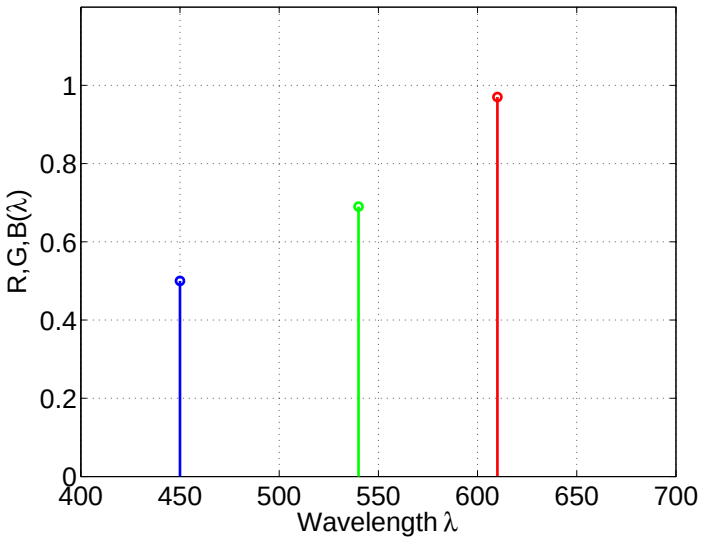

Figure 4.12: Ideal Delta function camera sensor gains

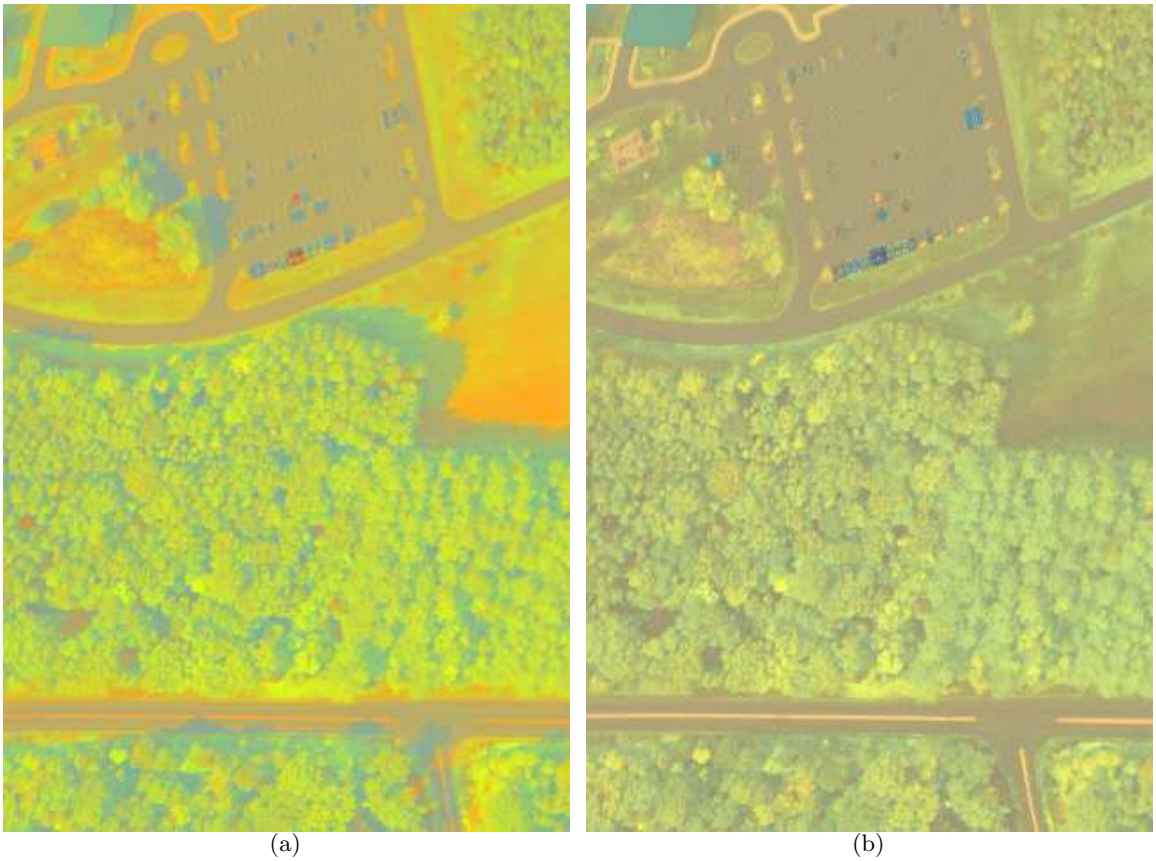

(a) (b)

Figure 4.13: (a) Original Beltsville image in chromaticity space (b) Result of the method in chromaticity space

in chromaticity space, one can compare them together. It is clear that in the resulting chromaticity image lots of shadows are completely removed, for example from roads, parking lots and the middle parts of the forest, or at least reduced to a great extent, such as top right of the forest.

Since chromaticity is the colour without magnitude sometimes it is hard to interpret. In order to have more interpretable outcome from the method we first move from 31-dimensional spectral space to XYZ space, and then to SRGB using simple matrix conversion. We then match the colour histogram of the output with the colour histogram of original image, and de-saturate the result. The outcome of this process is in Figure 4.14(b). To make comparison easier we put the original image in SRGB format, and the resulted original SRGB image is shown in Figure 4.14(a).

It should be mentioned that the process described above is not re-integration and we are not building the original image without shadows. Thus the images are not comparable pixel to pixel, instead it is just used to visualize the output in more understandable and interpretable form.

Results presented from Beltsville image data show that the method for multispectral images

(a) (b)

Figure 4.14: (a) Original Beltsville image in SRGB (b) Result of the method after histogram match function applied, in SRGB

will work well if we make a multispectral image from our hyperspectral image first, but the question is why should we use less information in order to make a illumination invariant image? Using the described approach we reduced our 360 channels to only 31 channels which means we have not used lots of available information, most beyond visibility for human beings.

To make use of all the available information, we can use an extended version of our method, with 360 channels instead of 31 which accepts 360-dimensional input data. The process as it sounds is computationally time-consuming, so we did that on a smaller patch of the image, the part which is most challenging in terms of strongest illumination effects. Figure 4.15 shows this part of input image data in SRGB.

As you can see, there are shadows on the road, as well as in parking lots and forest; the shadow in forest is very strong which makes it even harder to remove. If we apply our method to 360-dimensional data, the resulting chromaticity output would be in 360-dimensional space as well. In order to visualize that one can use the interpolation as we used in previous approach, cut the visible

Figure 4.15: Hyperspectral input image data , Beltsville data set.

domain and then visualize just that part of the spectrum. A result of such an approach is shown in Figure 4.16

As you can see, Figure 4.16(a) shows the chromaticity of original image, and Figure 4.16(b) shows the chromaticity of the resulting image, but the resulting image is not promising in terms of removing illumination effects. A valid question would be why this is happening when we are using more information than previous approach? Does this mean that our method can only work for multispectral images and not for hyperspectral images?

The answer is *"No"*. In fact the method works fine, the reason for a "not-good" result, a result where illumination effects are visually distinct, was mentioned before in §2.2. When we are dealing with hyperspectral images we should consider beyond visibility channels in visualizing the original or resulted image. Here we process all the channels in processing time, but when we try to visualize we only use the visible channels. If we take a closer look we can see that using whole spectrum, the method tries to remove illumination effects from all spectral channels, both in visible and invisible domain to a great extent. To show this we use information from two points in the image, one in the shadow and one in the light. Figure 4.17 shows two points; the blue one is in shadow while the red one is in the light.

The actual surface of those two points in the picture are similar so their spectrum after removing illumination should be similar, although their spectrum is not similar before removing illumination effects. Figure 4.18(a) shows the spectrum of those points before removing illumination effects and Figure 4.18(b) shows the spectrum after removing the illumination effects.

In the Figure 4.18(a) and (b), the green shaded area is the human visibility domain. It shows that the visible domain is small in comparison with the full spectral domain, and that although

(a)

(b)

Figure 4.16: (a) Original image in chromaticity space (b) Result in chromaticity space

the invariant spectrum of two points do not match exactly, the space between them is reduced greatly even in the visible domain. In general the result shows the effectiveness of our method for hyperspectral images to a great extent.

Another way to show the effectiveness of the proposed method is to visualize the full spectrum as an image. There have been many attempts for visualizing hyperspectral images which have been mentioned in §1.3. We used the method proposed by Jacobson and Gupta in [42] and extended by Jacobson et al. in [43]. In their work they proposed different envelopes, which can be used for visualization purposes. Here the Colour Matching Function Stretched is used. Figure 4.19 shows that function which is stretched to the whole spectra.

Using their method the resulting original image and resulting invariant image are shown in Figure 4.20. As you can see the illumination effects, such as shadow, are not removed completely but reduced to a great extent.

Figure 4.17: Two points in Beltsville hyperspectral image. Blue point is in shadow, Red point is in light.

4.3.2 AVIRIS f960628t01p02r04 Dataset

Another dataset used for testing the proposed method was from Airborne Visible/Infrared Imaging Spectrometer (AVIRIS) [52], dataset f960628t01p02r04 which was also used in [2] as well. This data set is huge, so we used 3 different patches from it. The dataset has 224 channels, which is less than the Beltsville dataset.

Similar to Beltsville dataset we first apply our method on AVIRIS f960628t01p02r04 dataset by making the ideal 31-dimensional interpolation of the hyperspectral data, and applying our method for multispectral images to it. The original image for three different patches of the dataset is shown in (a) of Figures 4.21, 4.22 and 4.23. The original chromaticities are in (b) of those Figures.

In Figure 4.21(c) the resulting chromaticity for illumination invariant image is shown. The strong shadows are removed very well. The same output for patch 2 and 3 of the dataset can be seen in Figure 4.22(c) and Figure 4.23(c).

Part (d) of AVIRIS result figures show the problem discussed in the Beltsville dataset, when we apply the hyperspectral method to whole spectrum but we show only the visible domain spectrum as output. The shadow is reduced but it is still there. We applied the same procedure as in the Beltsville dataset. We choose two points which should have similar surface reflectance, one in shadow and another in light. The chosen points are shown in part (a) of Figures 4.21, 4.22 and 4.23, where the red point is in light and the blue point is in shadow.

Plots shown in part (e) and (f) of AVIRIS result figures shows that although the method for hyperspectral images is not as successful as the method for multispectral imagel in removing

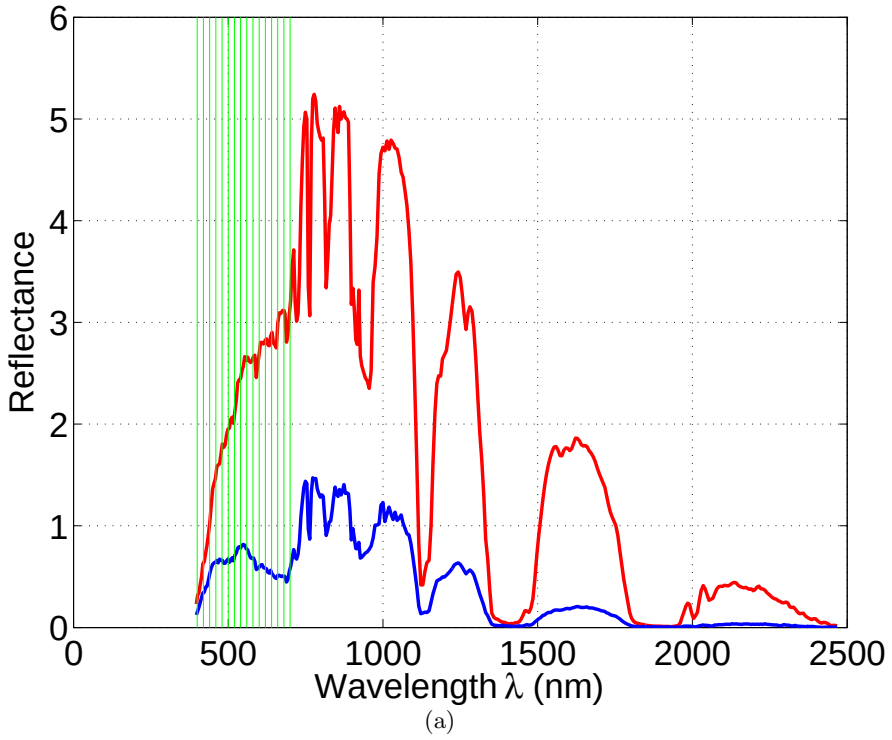

(a)

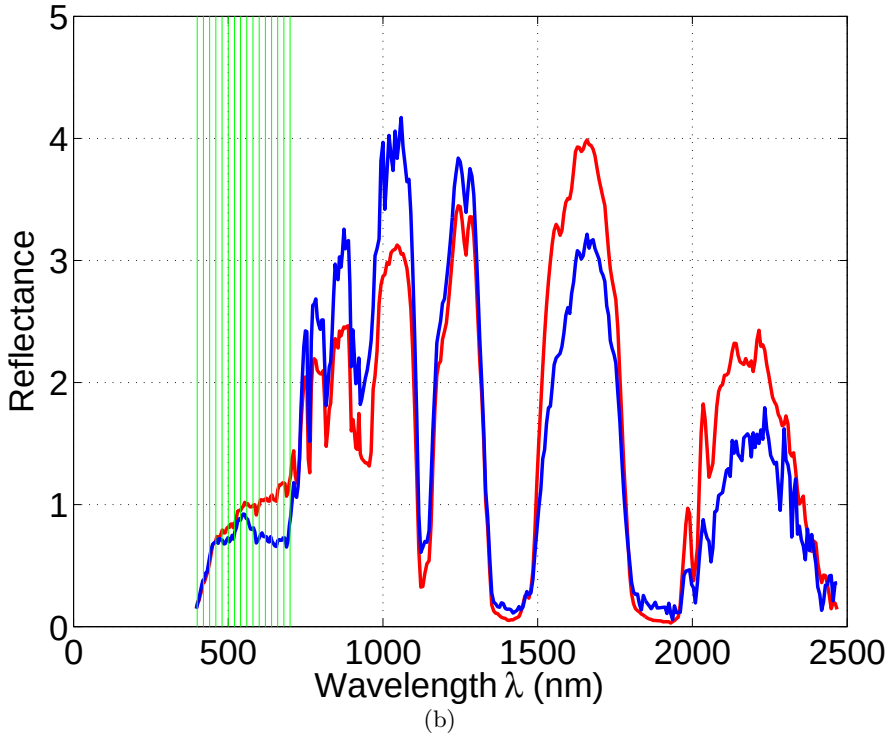

(b)

Figure 4.18: (a) Spectrum of shadow point (blue) and light point (red) in original image data (b) Spectrum of shadow point (blue) and light point (red) after applying illumination invariant method

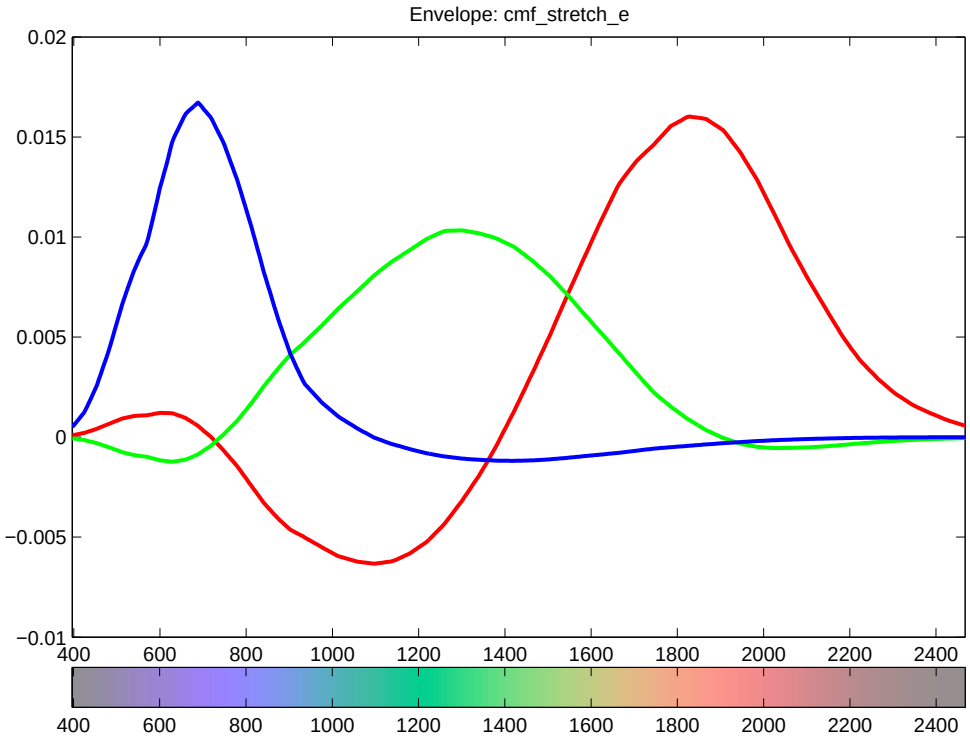

Figure 4.19: Colour Matching Function of CIELAB 1964 Stretched to whole spectra

illumination effects and the illumination effects are still visually distinct, it made the spectra look closer to each other than they were in the original image.

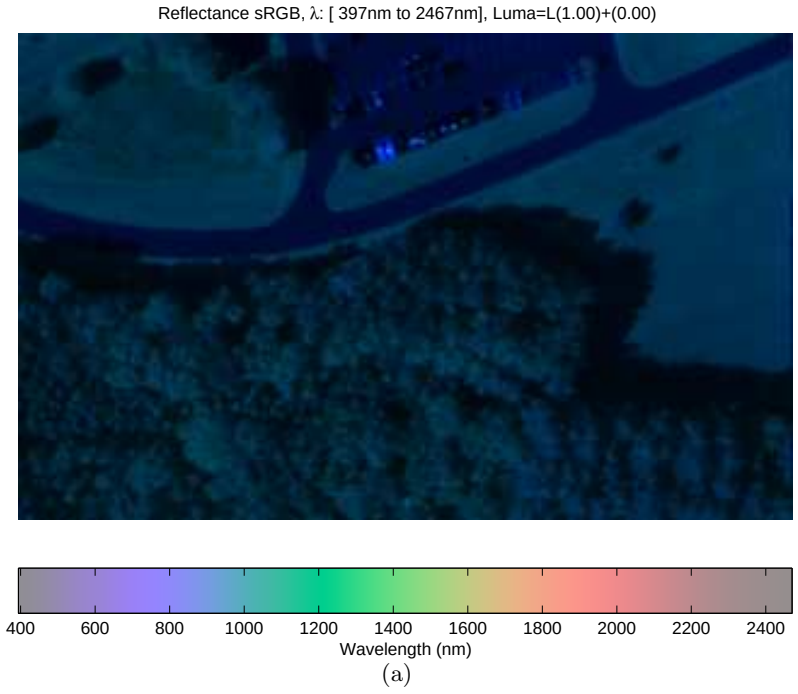

Figure 4.20: (a) Visualized Hyperspectral Original Image using CMF Stretched (b) Visualized Hyperspectral Illumination Invariant Image using CMF Stretched

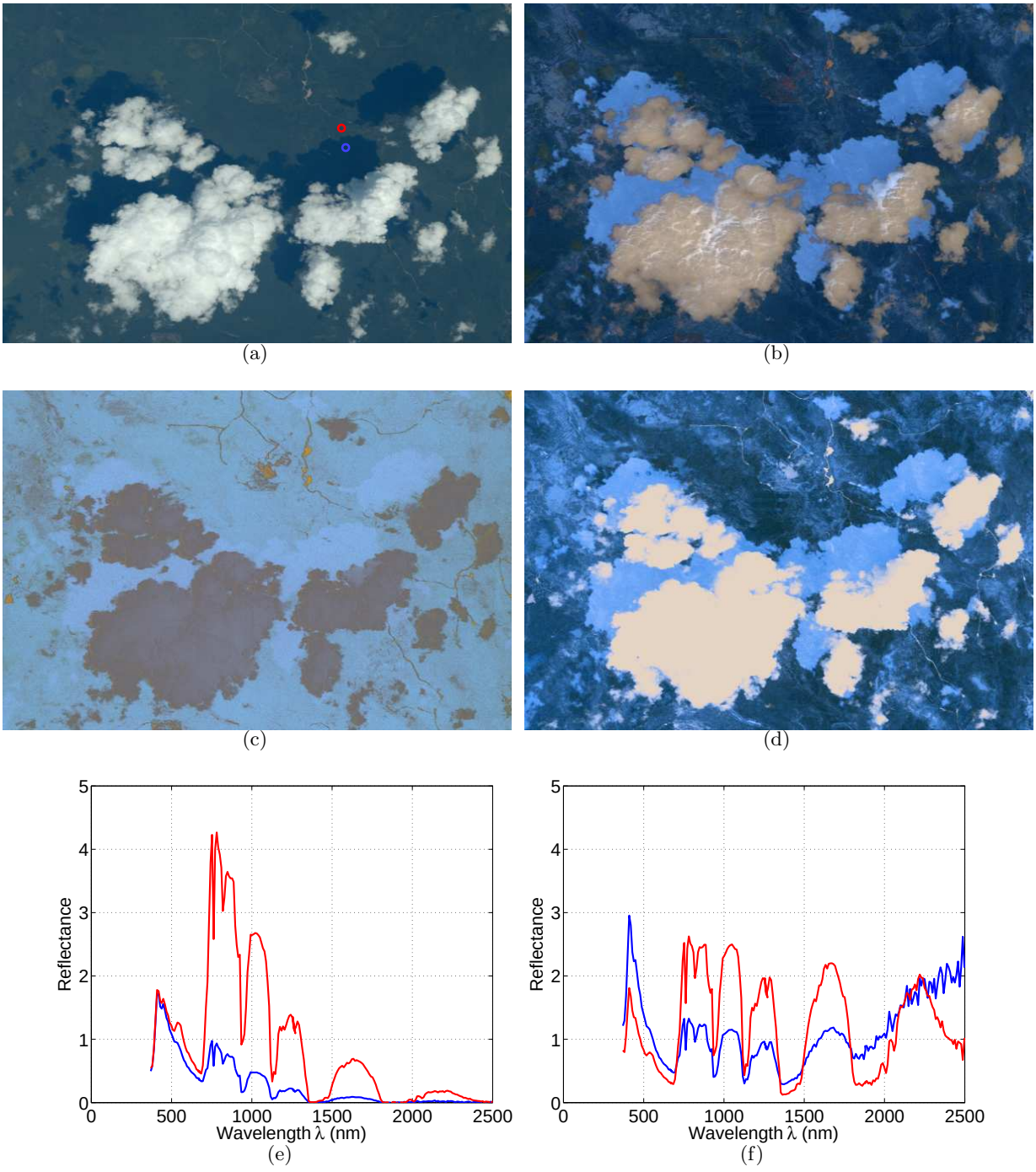

Figure 4.21: AVIRIS f960628t01p02r04 dataset, Patch1 : (a) Original Image in SRGB, Shadow point (blue) and light point (red) (b) Original Chromaticity Image (c) Invariant Image using visible spectrum (d) Invariant Image using whole spectrum (e) Original spectrum plot for red and blue points. Red is in light and blue is in shadow (f) Invariant spectrum plot for red and blue points. Red is in light and blue is in shadow

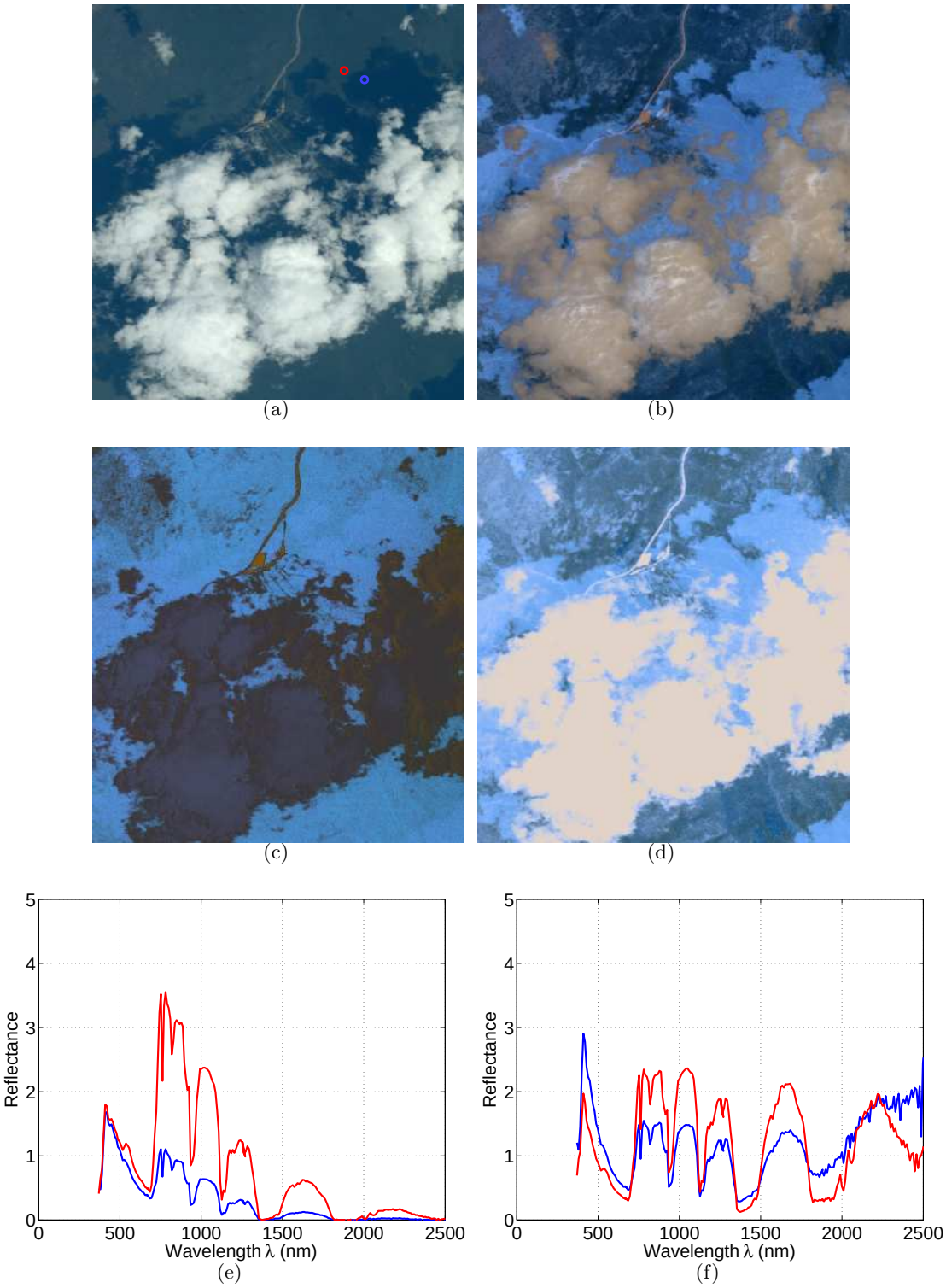

Figure 4.22: AVIRIS f960628t01p02r04 dataset, Patch2 : (a) Original Image in SRGB, Shadow point (blue) and light point (red) (b) Original Chromaticity Image (c) Invariant Image using visible spectrum (d) Invariant Image using whole spectrum (e) Original spectrum plot for red and blue points. Red is in light and blue is in shadow (f) Invariant spectrum plot for red and blue points. Red is in light and blue is in shadow

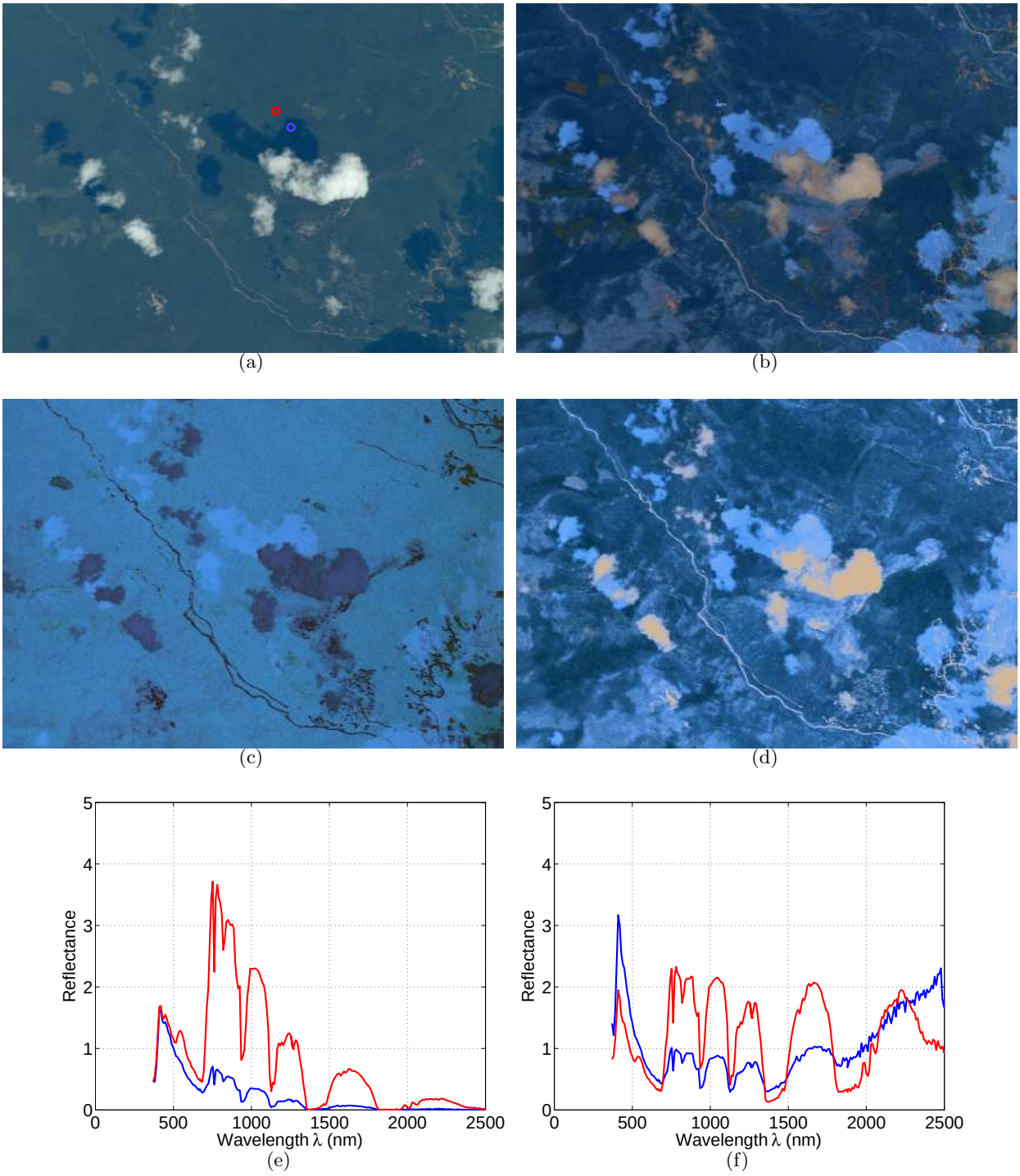

Figure 4.23: AVIRIS f960628t01p02r04 dataset, Patch3 : (a) Original Image in SRGB, Shadow point (blue) and light point (red) (b) Original Chromaticity Image (c) Invariant Image using visible spectrum (d) Invariant Image using whole spectrum (e) Original spectrum plot for red and blue points. Red is in light and blue is in shadow (f) Invariant spectrum plot for red and blue points. Red is in light and blue is in shadow

Chapter 5

Conclusion

5.1 Conclusion

In this thesis we have set out a method for producing an illumination-invariant spectral image. The method was to a good degree successful in removing effects of illuminant strength and colour, and of shading as well, for multispectral images. For hyperspectral images, however, the method was not completely successful in removing these illumination effects; some effects remain visually distinct. Nevertheless the method was successful in suppressing the effects to great extent.

My contribution in this work was partly in design of the method: discovery of the new method for finding an illumination-invariant direction in this new regime of images greater than 3-D; and also in implementing the method and doing experiments on different datasets. I also analyzed and interpreted the results to refine the method. The method was implemented using MATLAB.

I found that the task of removing the effects of illumination is significantly eased using spectral images, since the main objective, that of finding an illumination-invariant direction, easily falls out of the nature of the data – sensors are indeed narrowband and this makes this task relatively simple. I found that this results in images that are highly invariant to illumination, for multispectral images (here, using 31 channels). For hyperspectral images, however, with hundreds of spectral bands, results were not as promising as they were for multispectral images. Nonehtheless illumination effects are still suppressed.

Suppressing or removing illumination effects will help in many applications. For example in remote sensing, illumination effects can cause misclassification of the material in different regions but with using the illumination invariant method as a preprocessing step we might indeed be able to increase the accuracy of classification.

Another possible application of this method is in edge detection and segmentation. Illumination effects can cause extra edges in an image where there is no material change. These edges can cause

over-segmentation. By using the illumination invariant method we can improve the results of edge detection and segmentation.

The method still has some limitations. Specularities are seen to remain a problem for the method proposed. Of course, if we knew or measured the spectral function for the illuminant, then simple subtraction-based methods can in principle remove specularities: these methods customarily make the assumption that illumination is equi-energy, uniformly "white" across the spectrum [73] [62]. However, making use of the special knowledge of the illuminant spectrum is not in fact generating an illumination "invariant" – i.e., a quantity which is independent of lighting, without knowledge of the lighting; and indeed here we make no assumption about the lighting.

Discovering material mixtures that all contribute in each pixel is another problem still to be tackled. In hyperspectral images, usually each pixel may represent a mixture of several different materials. This can cause problems because the mix of those materials can reflect the light differently and this will lead to complications and finally poor results. Discovering mixtures is one of the chief aims of hyperspectral imaging, and using the method set out here in this important task is still an open question.

5.2 Future Work

Possible work in future work could be focusing on specularities. One can address this issue by examining schemes for determining the spectral-gain offset vector $\log \phi_k$, and hence in effect the specular point. If the spectral point is known in the 31-dimensional multispectral space or in higher-dimensional hyperspectral space, matte colours might be determined by knowing to what extent specular content is included in spectral image pixel data.

Another direction for future work can be to examine how breaking the assumption of narrow-band sensors, and using broader-band sensors, would affect the invariant generated here. Another approach could be to apply spectral sharpening to such broader-band sensors. As well, the model used assumes a Planckian light, whereas the experiments in § 4.2 with real data use standard day-lights in a light-box. The question remains, then, to what degree departing from the Planckian model affects results in general.

One other direction can be re-integrating using the gradient information from the chromaticity image and spectral information from the original image, and re-building the original hyperspectral image but without illumination effects. The resulting image in original space might be used for determining the material in hyperspectral images with higher accuracy, without illumination effects.

Testing the effectiveness of the method for other applications such as segmentation and edge detection is another possible way to extend this work.

Bibliography

[1] S.M. Adler-Golden, R.Y. Levine, M.W. Matthew, S.C. Richtsmeier, L.S. Bernstein, J.H. Gruninger, G.W. Felde, M.L. Hoke, G.P. Anderson, and A. Ratkowski. Shadow-insensitive material detection/classification with atmospherically corrected hyperspectral imagery. volume 4381, pages 460–469. SPIE, 2001.

[2] S.M. Adler-Golden, M.W. Matthew, G.P. Anderson, G.W. Felde, and J.A. Gardner. Algorithm for de-shadowing spectral imagery. In S. S. Shen, editor, *Society of Photo-Optical Instrumentation Engineers (SPIE) Conference Series*, volume 4816 of *Society of Photo-Optical Instrumentation Engineers (SPIE) Conference Series*, pages 203–210, September 2002.

[3] E.A. Ashton, B.D. Wemett, R.A. Leathers, and T.V. Downes. A novel method for illumination suppression in hyperspectral images. volume 6966, page 69660C. SPIE, 2008.

[4] H. G. Barrow and J. M. Tenenbaum. Recovering intrinsic scene characteristics from images. In Hanson and Riseman, editors, *Computer Vision Systems*, pages 3–26, New York, New York, 1978. Academic Press.

[5] M. Brown and S. Süsstrunk. Multispectral SIFT for scene category recognition. In *Computer Vision and Pattern Recognition (CVPR11)*, pages 177–184, Colorado Springs, June 2011.

[6] S. Cai, Q. Du, and R. J. Moorhead. Hyperspectral imagery visualization using double layers. *IEEE Trans. Geoscience and Remote Sensing*, 45(10):3028–3036, October 2007.

[7] International Electrotechnical Commission. Multimedia systems and equipment – colour measurement and management – part 2-1: Colour management – default RGB colour space – sRGB. IEC 61966-2-1:1999.

[8] C. de Boor. *A Practical Guide to Splines*. Number 27 in Applied Mathematical Sciences. Springer-Verlag, New York, 1978.

[9] M. S. Drew and G. D. Finlayson. Recovery of chromaticity image free from shadows via illumination invariance. In *In IEEE Workshop on Color and Photometric Methods in Computer Vision, ICCV03*, pages 32–39, 2003.

[10] M. S. Drew and A. Yazdani Salekdeh. Multispectral image invariant to illumination colour, strength, and shading. In *Digital Photography VII*, pages 78760A1–9. SPIE, 2011.

[11] M. S. Drew, J. Wei, and Z. N. Li. Illumination-invariant color object recognition via compressed chromaticity histograms of color-channel-normalized images. In *ICCV*, pages 533–540, 1998.

[12] Q. Du, N. Raksuntorn, S. Cai, and R. J. Moorhead. Color display for hyperspectral imagery. *IEEE Trans. Geoscience and Remote Sensing*, 46(6):1858–1866, June 2008.

[13] R. Erbacher, D. Gonthier, and H. Levkowitz. The color icon: A new design and a parallel implementation. In *Proceedings of the SPIE '95 Conference on Visual Data Exploration and Analysis II*, pages 302–312, 1995.

[14] G. D. Finlayson, S. S. Chatterjee, and B. V. Funt. Color angular indexing. In *ECCV*, pages II:16–27, 1996.

[15] G. D. Finlayson and M. S. Drew. 4-sensor camera calibration for image representation invariant to shading, shadows, lighting, and specularities. In *Proceedings of the Eighth International Conference On Computer Vision (ICCV-01)*, pages 473–480, Los Alamitos, CA, July 9–12 2001. IEEE Computer Society.

[16] G. D. Finlayson, M. S. Drew, and B. V. Funt. Spectral sharpening: Sensor transformations for improved color constancy. *Journal of the Optical Society of America*, 11(5):1553–1563, May 1994.

[17] G. D. Finlayson, M. S. Drew, and C. Lu. Intrinsic images by entropy minimization. In Tomás Pajdla and Jiri Matas, editors, *ECCV (3)*, volume 3023 of *Lecture Notes in Computer Science*, pages 582–595. Springer, 2004.

[18] G. D. Finlayson, M. S. Drew, and C. Lu. Entropy minimization for shadow removal. *International Journal of Computer Vision*, 85(1):35–57, 2009.

[19] G. D. Finlayson and S. D. Hordley. Color constancy at a pixel. *Journal of the Optical Society of America*, 18(2):253–264, February 2001.

[20] G. D. Finlayson, S. D. Hordley, and M. S. Drew. Removing shadows from images. In Anders Heyden, Gunnar Sparr, Mads Nielsen, and Peter Johansen, editors, *ECCV (4)*, volume 2353 of *Lecture Notes in Computer Science*, pages 823–836. Springer, 2002.

[21] G. D. Finlayson, S. D. Hordley, and P. M. Hubel. Color by correlation: A simple, unifying framework for color constancy. *IEEE Trans. Pattern Anal. Mach. Intell*, 23(11):1209–1221, 2001.

[22] G.D. Finlayson. Color in perspective. *Pattern Analysis and Machine Intelligence, IEEE Transactions on*, 18(10):1034 –1038, October 1996.

[23] G.D. Finlayson, S.D. Hordley, Cheng Lu, and M.S. Drew. On the removal of shadows from images. *Pattern Analysis and Machine Intelligence, IEEE Transactions on*, 28(1):59 –68, 2006.

[24] D. A. Forsyth. A novel algorithm for color constancy. *International Journal of Computer Vision*, 5(1):5–36, August 1990.

[25] J. Franklin, T.L. Logan, C.E. Woodcock, and A.H. Strahler. Coniferous forest classification and inventory using landsat and digital terrain data. *Geoscience and Remote Sensing, IEEE Transactions on*, GE-24(1):139 –149, 1986.

[26] W. T. Freeman and P. A. Viola. Bayesian model of surface perception. In Michael I. Jordan, Michael J. Kearns, and Sara A. Solla, editors, *Advances in Neural Information Processing Systems*, volume 10. The MIT Press, 1998.

[27] B. V. Funt, M. S. Drew, and M. Brockington. Recovering shading from color images. In *Computer Vision – ECCV 92*, pages 124–132, Santa Margherita Ligure, Italy, 19–22 May 1992. Springer-Verlag.

[28] B. V. Funt and G. D. Finlayson. Color constant color indexing. *IEEE Trans. Pattern Analysis and Machine Intelligence*, 17(5):522–529, May 1995.

[29] P.M. Morovic G.D. Finlayson and S.D. Hordley. Using the spectracube to build a mulitspectral image database. pages 268–274, 2004.

[30] T. Gevers and A. W. M. Smeulders. Color-based object recognition. *Pattern Recognition*, 32(3):453–464, March 1999.

[31] T. Gevers and H. M. G. Stokman. Classifying color transitions into shadow-geometry, illumination, highlight or material edges. In *ICIP*, pages Vol I: 521–524, 2000.

[32] M. R. Gupta and N. P. Jacobson. Wavelet principal component analysis and its application to hyperspectral images. In *ICIP*, pages 1585–1588, 2006.

[33] X. D. He, K. E. Torrance, F. X. Sillion, and D. P. Greenberg. A comprehensive physical model for light reflection. *SIGGRAPH Comput. Graph.*, 25:175–186, July 1991.

[34] C. G. Healey and J. T. Enns. Large datasets at a glance: Combining textures and colors in scientific visualization. *IEEE Transactions on Visualization and Computer Graphics*, 5(2):145–167, April/June 1999.

[35] G. Healey and D. A. Slater. Models and methods for automated material indentification in hyperspectral imagery acquired under unknown illumination and atmospheric conditions. *IEEE Trans. Geoscience and Remote Sensing*, 37(6):2707–2717, November 1999.

[36] G. Healey and L. Z. Wang. Illumination-invariant recognition of texture in color images. *Journal of the Optical Society of America*, 12(9):1877–1883, September 1995.

[37] S. Hordley, G. D. Finalyson, and P. Morovic. A multi-spectral image database and its application to image rendering across illumination. In *Image and Graphics, 2004. Proceedings. Third International Conference on*, pages 394 – 397, 2004.

[38] B. K. P. Horn. Determining lightness from an image. *Computer Graphics and Image Processing*, 3(1):277–299, December 1974.

[39] R. L. Hsu, M. Abdel Mottaleb, and A. K. Jain. Face detection in color images. *IEEE Trans. Pattern Analysis and Machine Intelligence*, 24(5):696–706, May 2002.

[40] A. Hurlbert. Formal connections between lightness algorithms. *J. Opt. Soc. Am. A*, 3(10):1684–1693, Oct 1986.

[41] C. R. Jung J. C. S. Jacques and S. R. Musse. Background subtraction and shadow detection in grayscale video sequences. In *SIBGRAPI*, pages 189–196. IEEE Computer Society, 2005.

[42] N. P. Jacobson and M. R. Gupta. Design goals and solutions for display of hyperspectral images. *IEEE Trans. Geoscience and Remote Sensing*, 43(11):2684–2692, November 2005.

[43] N. P. Jacobson, M. R. Gupta, and J. B. Cole. Linear fusion of image sets for display. *IEEE Trans. Geoscience and Remote Sensing*, 45(10):3277–3288, October 2007.

[44] O. Javed and M. Shah. Tracking and object classification for automated surveillance. In *ECCV*, page IV: 343 ff., 2002.

[45] C. Jaynes, S. Webb, and R. M. Steele. Camera-based detection and removal of shadows from interactive multiprojector displays. *IEEE Transactions on Visualization and Computer Graphics*, 10(3):290–301, May/June 2004.

[46] C. Jaynes, S. Webb, R. M. Steele, M. Brown, and W. B. Seales. Dynamic shadow removal from front projection displays. *Visualization Conference, IEEE*, 0:null, 2001.

[47] G.M. Johnson and M.D. Fairchild. Full-spectral color calculations in realistic image synthesis. *Computer Graphics and Applications*, 19(4: July/August):47–53, 1999.

[48] D. Judd, D. MacAdam, and G. Wyszecki. Spectral distribution of typical daylight as a function of correlated color temperature. *Journal of the Optical Society of America*, 54(8):1031–1040, 1964.

[49] J. T. Kajiya. Anisotropic reflection models. *SIGGRAPH Comput. Graph.*, 19:15–21, July 1985.

[50] S. Kawato and J. Ohya. Real-time detection of nodding and head-shaking by directly detecting and tracking the 'between-eyes'. In *FG*, pages 40–45, 2000.

[51] G.J. Klinker, S.A. Shafer, and T Kanade. A physical approach to color image understanding. *International Journal of Computer Vision*, 4:7–38, 1990.

[52] Jet Propulsion Laboratory. Aviris dataset, flight date: 28/06/96, 2011.

[53] E. H. Land. The retinex theory of color vision. *Scientific American*, 237(6):108–128, December 1977.

[54] E. H. Land and J. J. McCann. Lightness and retinex theory. *Journal of the Optical Society of America*, 61(1):1–11, 1971.

[55] H. C. Lee, E. J. Breneman, and C. P. Schulte. Modeling light reflection for computer color vision. *IEEE Trans. Pattern Analysis and Machine Intelligence*, 12(4):402–409, April 1990.

[56] Z.-N. Li and M.S. Drew. *Fundamentals of Multimedia*. Prentice-Hall, 2004.

[57] SpecTIR LLC. Agriculture and vegetation sample: Beltsville, md, usa, 2011.

[58] R. S. Longhurst. *Geometrical and Physical Optics*. Longman, London, 1967.

[59] L. T. Maloney and B. A. Wandell. Color constancy: A method for recovering surface spectral reflectance. *Journal of the Optical Society of America*, 3:29–33, 1986.

[60] J. C. Maxwell. A dynamical theory of the electromagnetic field. *Philosophical Transactions of the Royal Society of London*, 155:459–513, 1865.

[61] C.S. McCamy, H. Marcus, and J.G. Davidson. A color-rendition chart. *J. Appl. Photogr. Eng.*, 2(3):95–99, Summer 1976.

[62] R. Montoliu, F. Pla, and A. C. Klaren. Illumination intensity, object geometry and highlights invariance in multispectral imaging. In *Iberian Conference on Pattern Recognition and Image Analysis*, page I:36, 2005.

[63] B. T. Phong. Illumination for computer generated pictures. *Communications of the ACM*, 18(6):311–317, 1975.

[64] K. Ranson and C. T. Daughtry. Scene Shadow Effects on Multispectral Response. *IEEE Transactions on Geoscience and Remote Sensing*, 25:502–509, July 1987.

[65] P. Ready and P. Wintz. Information extraction, snr improvement, and data compression in multispectral imagery. *Communications, IEEE Transactions on*, 21(10):1123 – 1131, October 1973.

[66] R. Richter. De-Shadowing of Satellite/Airborne Multispectral and Hyperspectral Imagery. October 2005.

[67] C. Runge. Ueber empirische Funktionen und die Interpolation zwischen aequidistanten Ordinaten. *ZAMM*, 46:224–243, 1901.

[68] E. Salvador, A. Cavallaro, and T. Ebrahimi. Shadow identification and classification using invariant color models. In *ICASSP01*, pages 1545–1548, 2001.

[69] E. Salvador, A. Cavallaro, and T. Ebrahimi. Cast shadow segmentation using invariant color features. *Computer Vision and Image Understanding*, 95(2):238–259, August 2004.

[70] A. Schuster. *An Introduction to the Theory of Optics*. 1909.

[71] S.M. Singh and A.P. Cracknell. Effect of shadows cast by vertical protrusions on AVHRR data. *International Journal of Remote Sensing*, 6:1767–1771, November 1985.

[72] J. Stauder, R. Mech, and J. Ostermann. Detection of moving cast shadows for object segmentation. *IEEE Transactions on Multimedia*, 1(1):65–76, March 1999.

[73] H. M. G. Stokman and T. Gevers. Detection and classification of hyper-spectral edges. In *BMVC*, pages Low and High–Level Feature Detection, 1999.

[74] P. H. Suen and G. Healey. Invariant mixture recognition in hyperspectral images. In *ICCV*, pages I: 262–267, 2001.

[75] R. Sukthankar, T. J. Cham, and G. Sukthankar. Dynamic shadow elimination for multi-projector displays. In *CVPR*, pages II:151–157, 2001.

[76] Y. Sun, F.D. Fracchia, M.S. Drew, and T.W. Calvert. Rendering iridescent colors of optical disks. In *11th Eurographics Workshop on Rendering*, pages 341–352, June 26-28, Brno, Czech Republic 2000.

[77] J. S. Tyo, A. Konsolakis, D. I. Diersen, and R. C. Olsen. Principal-components-based display strategy for spectral imagery. *IEEE Trans. Geoscience and Remote Sensing*, 41(3):708–718, March 2003.

[78] Y. Weiss. Deriving intrinsic images from image sequences. In *Proceedings of the Eighth International Conference On Computer Vision (ICCV-01)*, pages 68–75, Los Alamitos, CA, July 9–12 2001. IEEE Computer Society.

[79] G. Wyszecki and W. S. Stiles. *Color Science: Concepts and Methods, Quantitative Data and Formulae*. Wiley, 1982.

[80] J. Yang and A. Waibel. A real-time face tracker. In *WACV*, pages 142–147, 1996.

[81] J. Ye, T. Wittman, X. Bresson, and S. Osher. Segmentation for hyperspectral images with priors. In *Advances in Visual Computing - 6th International Symposium, ISVC 2010*, volume 6454 of *Lecture Notes in Computer Science*, pages 97–106. Springer, 2010.

[82] X. Zhang and B. A. Wandell. A spatial extension of CIELAB for digital color image reproduction, October 09 1996.